Flinders University

Hydrogeological conceptual model and numerical groundwater flow model of the Northern Adelaide Corridor

By

Marcos Davalos Gutierrez

Thesis
Submitted to Flinders University
for the degree of Master of Science in Groundwater Hydrology

Master of Science: Groundwater Hydrology

College of Science and Engineering
Submitted May 24th and amended July 19th, 2024.

TABLE OF CONTENTS

ABSTRACT

The Northern Adelaide Corridor (NAC), South Australia, has potential to sustain groundwater irrigated agriculture, however, little is known about its hydrogeology since groundwater extraction is limited and it's not in a prescribed wells area. A conceptual model and a numerical groundwater model were developed for the NAC to identify its main hydrogeological units, estimate their hydraulic conductivities and water balances, as well as to approximate a steady-state water table. The conceptual model is based on previous studies of the area or nearby and on the analysis of various environmental features such as topography, geology, and climate. The numerical groundwater flow model is based upon the conceptual model and was developed using the graphical user interface ModelMuse for MODFLOW-NWT. The numerical model is steady-state and incorporates different types of data such as topographic data, bore stratigraphic records, records from stream gauges, precipitation, evapotranspiration, and hydraulic head observations from monitoring networks and measured in-situ. The simulation of the calibrated numerical model allowed the computation of the hydraulic head distribution, the determination of the general direction of groundwater flow, estimate the water balances of the hydrostratigraphic units, and estimate the travel times of water particles given specific pathlines. Despite some significant data gaps encountered, the numerical model performed relatively well with a Root Mean Squared Residual (RMSR) of 2.52 m and provided a good conceptual model candidate that can be further refined.

DECLARATION

I certify that this thesis does not incorporate without acknowledgment any material previously submitted for a degree or diploma in any university; and that to the best of my knowledge and belief it does not contain any material previously published or written by another person except where due reference is made in the text.

Signed: Marcos Davalos Gutierrez

Date: May 24th, 2024

ACKNOWLEDGEMENTS

I want to thank my supervisors Eddie Banks, Daniel Partington and Okke Batelaan, for their continued support, guidance and encouragement. I learned a lot from you and from this project. I also want to thank Steve Barnett from the Department for Environment and Water for his assistance. Thanks to all the teachers I had while studying at Flinders University.

Lastly, I would like to thank my family and friends back home for their love and support despite the distance, as well as the wonderful people I met while studying this degree for their unconditional support. This wouldn't have been possible without any of you.

LIST OF FIGURES

LIST OF TABLES

1. INTRODUCTION

The Northern Adelaide Corridor (NAC) located north of Adelaide between the Gawler and Wakefield rivers stands poised for economic growth through expansion of horticulture, with groundwater resources playing a pivotal role. In a comprehensive assessment conducted by the Goyder Institute for Water Research, spanning from the Gawler to Wakefield Rivers (see Figure 1), viable surface water and groundwater sources were explored that could drive economic development in the region. The assessment highlighted a critical challenge: accessibility to high-quality water that would meet the requirements for agriculture. This issue holds particular significance in the context of South Australia's Growth State Plan, which aims for an ambitious 3% annual growth in Gross State Product (GSP), with primary industries serving as key contributors (Government of South Australia, 2022). Focused on the region between Mallala and Balaklava, there are reasonable quantities of groundwater, yet uncertainties persist regarding the suitability and sustainability. To ensure the success of the Growth State Plan, it becomes imperative to address these uncertainties through analysis of the water balance and water quality to support with facilitating sustainable water use practices.

Despite estimations of large groundwater quantities in the NAC region, critical knowledge gaps persist which require addressing. Notably, inadequate knowledge about the water balance and quality of water available throughout the year, lack of data on the depth to shallow (often saline) groundwater, and uncertainties related to how expanded irrigation might affect saline recharge and impact water quality are key concerns.

1.1 Objectives

This thesis line of research is focused on increasing the hydrogeological knowledge of the NAC, building on previous studies and readily available information to develop a conceptual model and a numerical groundwater flow model of the region. Specifically, this project will improve the hydrogeological conceptual model of the NAC region by performing an integrated analysis of the hydrostratigraphy, climatic and other environmental data up to date, develop a numerical model of the NAC using the graphical user interface ModelMuse for MODFLOW, approximate a steady-state hydraulic head distribution, estimate hydraulic conductivities and water balances of the hydrogeological units, and estimate water particles travel times.

1.2 Background and study area delineation

Previous groundwater studies of the Northern Adelaide Plains (NAP) (Goyder Institute Technical Report Series No. 12/x, 16/15 and 19/17) used the Light River as the northern boundary (Figure 1). For this study, the Light River was set to be the southern boundary to extend the hydrogeological

studies north, where information is scarcer. The northern boundary was defined to be the Wakefield River and the western boundary was the coast. The Alma Fault was selected to be the eastern boundary to comprise the longitudinal (East – West) extent of the Tertiary units and the transition from those units to the basement to study their potential interactions. The study area resulted to be of 1,738.51 km^2 and was denominated the Northern Adelaide Corridor (NAC) for this study (Figure 2).

Figure removed due to copyright restriction.

Figure 1. Study area of the Northern Adelaide Plains Water Stocktake. The area inside the red polygon was the main study area (the NAP) and has significantly more information available than the secondary study area (the area within the orange dashed line) especially north to it (The Goyder Institute for Water Research, 2016).

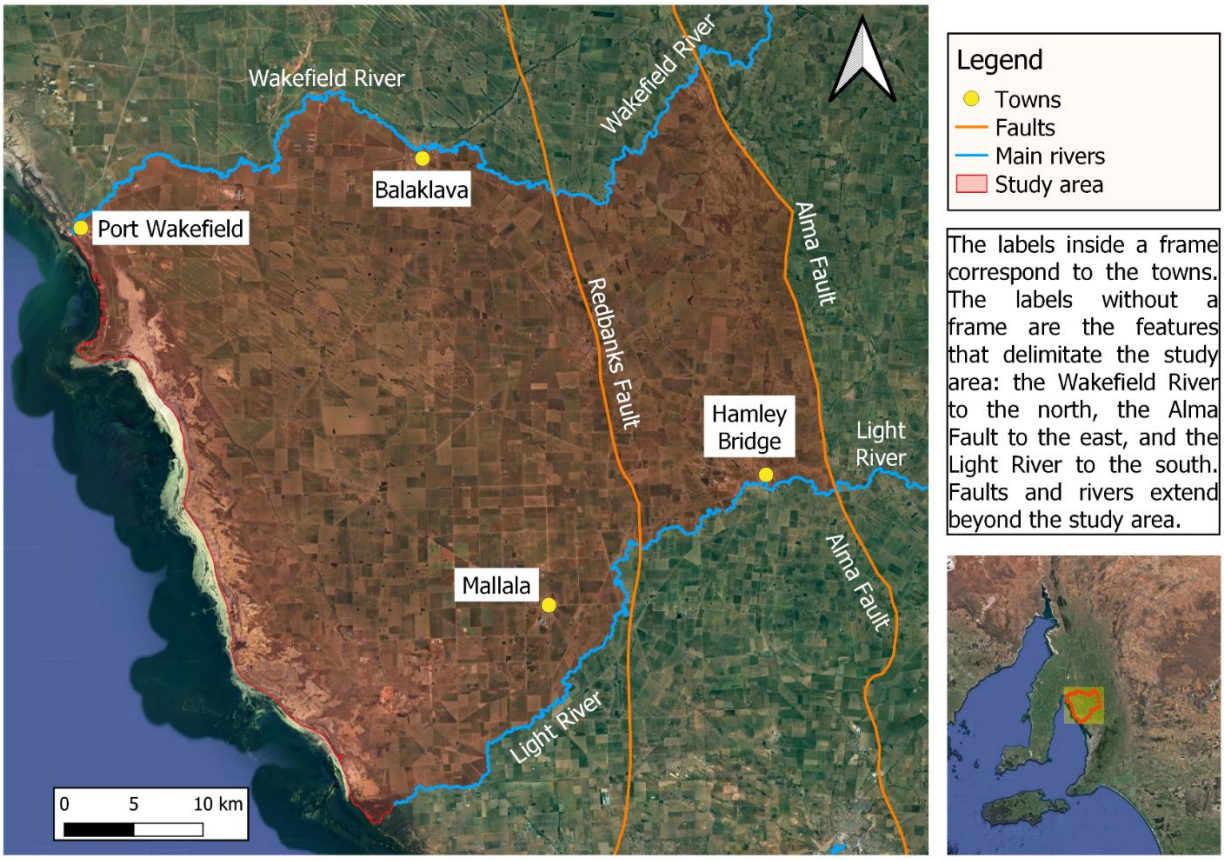

Figure 2. Study area (Northern Adelaide Corridor).

1.3 Topography

The digital elevation map (DEM) utilised in the work is the SRTM-derived Smoothed 1 Second Digital Elevation Model Version 1.0 obtained from Geosciences Australia at https://elevation.fsdf.org.au/. The DEM was clipped to the study area. The DEM highlights the mostly flat area of the coast moving east until reaching the Mount Lofty Ranges at around the 270,000 m Easting (approximately where the Redbanks Fault lies) at which point the large changes in elevation are evident (see Figure 3).

Figure removed due to copyright restriction.

Figure 3. Digital Elevation Map of the study area (Partington *et al.*, 2024).

1.4 Precipitation

Gridded monthly rainfall from 2000 to 2022 across the NAC was accessed and downloaded from SILO (https://www.longpaddock.qld.gov.au/silo/gridded-data/), downscaled to a 50 m by 50 m grid through a Python Jupyter notebook and then resampled to annual rainfall for that period. Figure 4 shows the spatio-temporal distribution of rainfall across the NAC. In each subplot the increasing rainfall away from the coast from east to west with a peak in the eastern MLR part of the NAC is evident. The high rainfall years of 2010, 2016 and 2022 are also clear as well as the very dry 2002, 2006, 2018 and 2019.

Figure removed due to copyright restriction.

Figure 4. Annual rainfall from 2000 to 2022 across the NAC (Partington *et al.*, 2024).

1.5 Land Use

Land use data for the NAC area was obtained from WaterConnect at http://www.waterconnect.sa.gov.au/Content/Downloads/DEWNR/LANDSCAPE_LandUse_ALUM_shp.zip. As seen in Figure 5, land use across the area is dominated by dryland agricultural use (cropping and grazing modified pastures). The cropping consists mostly of cereals (48% of the total area).

Figure removed due to copyright restriction.

Figure 5. Land use across the NAC (Partington et al., 2024).

1.6 Geology

The main geological units in the study area are (in sequence from top to bottom; youngest to oldest) the Hindmarsh Clay, Carisbrooke Sand, Port Willunga Formation, Rogue Formation, and Clinton Formation. The first two belong to the Quaternary period (2.6 million years ago to present) while the other three span from the Paleogene to the Neogene (55.8 to 2.6 million years ago) (Smith *et al*, 2015) or what was used to be called the Tertiary period.

The Hindmarsh Clay (HC) is the topmost layer of the study area composed of firm, sub-plastic clay with silty and fine to coarse–grained sand and gravel lenses (Smith *et al*, 2015). It extends over all the study area except in some small zones where the basement outcrops.

The Carisbrooke Sand (CS) is a fluvial, fossil-poor, cross-bedded, medium to coarse quartz sand with minor silt and clay (Smith *et al*, 2015). It usually underlies the Hindmarsh Clay, but it doesn't cover as much area as the Hindmarsh Clay.

The Port Willunga Formation (PW) is mainly a bryozoal marly limestone (Smith *et al*, 2015). It underlies the Hindmarsh Clay or the Carisbrooke Sand if present. The Port Willunga Formation is restricted to the southwest and west parts of the study area.

The Rogue Formation (RF) comprises sparsely fossiliferous, marginal-marine quartz sand and sandstone with minor limestone, mudstone and clay (Smith *et al*, 2015). This formation is below the Port Willunga Formation (where present), or the Hindmarsh Clay or CS (where the PW is not present). The Rogue Formation doesn't extend past the Redbanks Fault.

The Clinton Formation (CF) is characterised by lignite, carbonaceous clay, silt and sand. Lignite deposits are restricted to the northern part of the study area, where the formation is around 70 m thick, and comprises interbedded sand, silt, clay and lignite (Smith *et al*, 2015). It is underneath the Rogue Formation and, just like that one, it doesn't go beyond the Redbanks Fault.

The basement is usually below the Clinton Formation and it's composed of rocks from the Permian (299 to 251 million years ago) and Neoproterozoic (1000 to 541 million years ago) periods. Beyond the Redbanks Fault, the basement underlies the Hindmarsh Clay. The types of rocks found at the basement include siltstone, quartzite, shale, granite and slate.

Many cross sections were reported in the regional hydrogeological characterisation of the Saint Vincent Basin by Smith *et al* (2015) (Figure 6) and three of those are within the NAC. These are shown in figures 7 to 9.

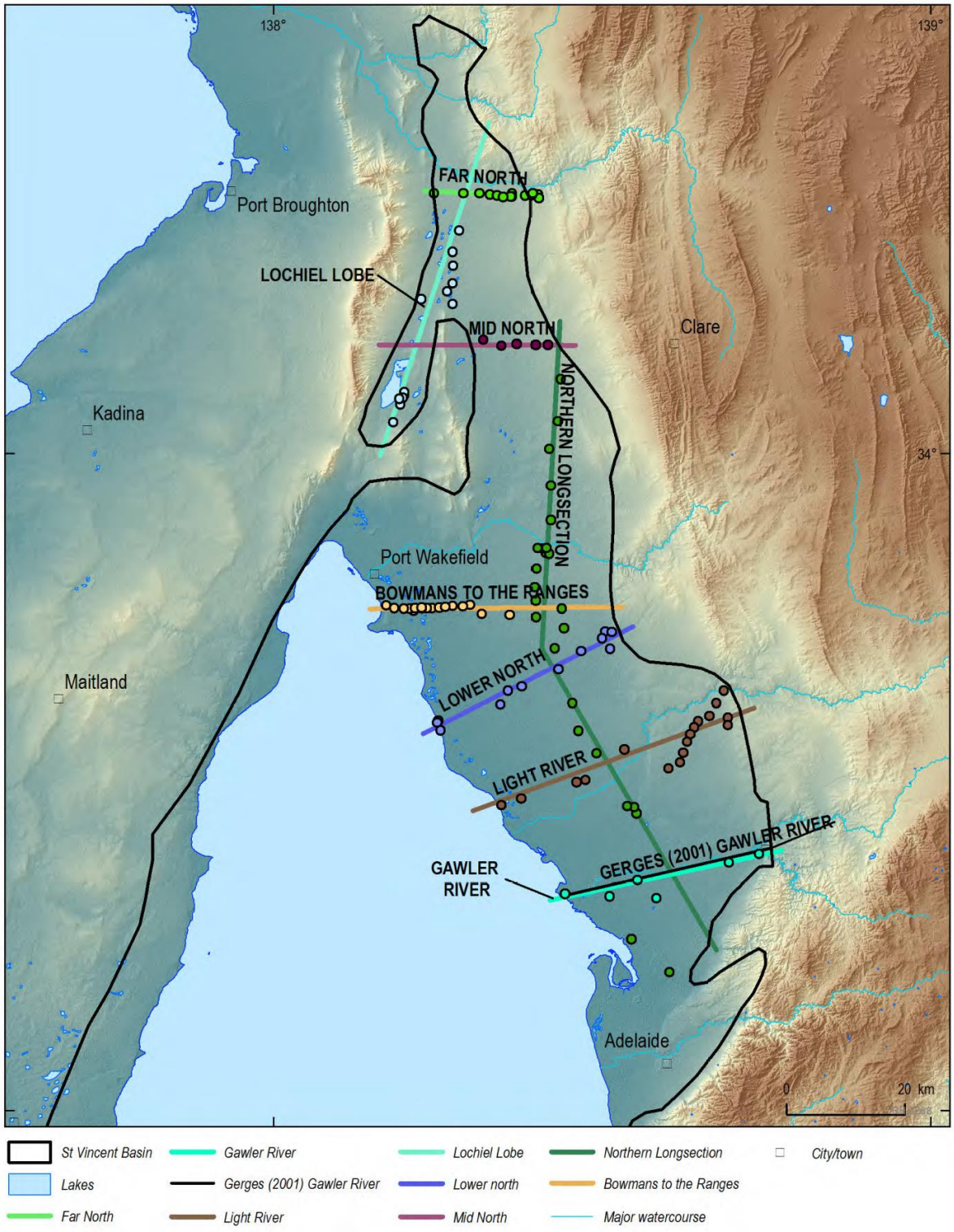

Figure 6. Location of schematic cross-sections and drillholes (coloured dots) used to inform interpretation (Smith *et al*, 2015, licensed under CC BY 4.0).

The cross sections shown in this document are “Bowmans to the ranges” (Figure 7), “lower north” (Figure 8) and a transect of the “northern long section” (Figure 9). With respect to the NAC, the Bowmans to the ranges is located in the northern portion of it, around 10 km south from the Wakefield River. Both the lower north and the transect of the northern long section are located at the centre of

the NAC, the former stretching east to west and the latter north to south. They were particularly useful for the development of the hydrogeological conceptual model of the area.

In Figure 7 it can be appreciated how the Port Willunga Formation ends halfway and transitions to the Rogue Formation. Nonetheless, a portion of the Rogue Formation goes underneath the Port Willunga before the complete transition. The Carisbrooke Sand barely appears here.

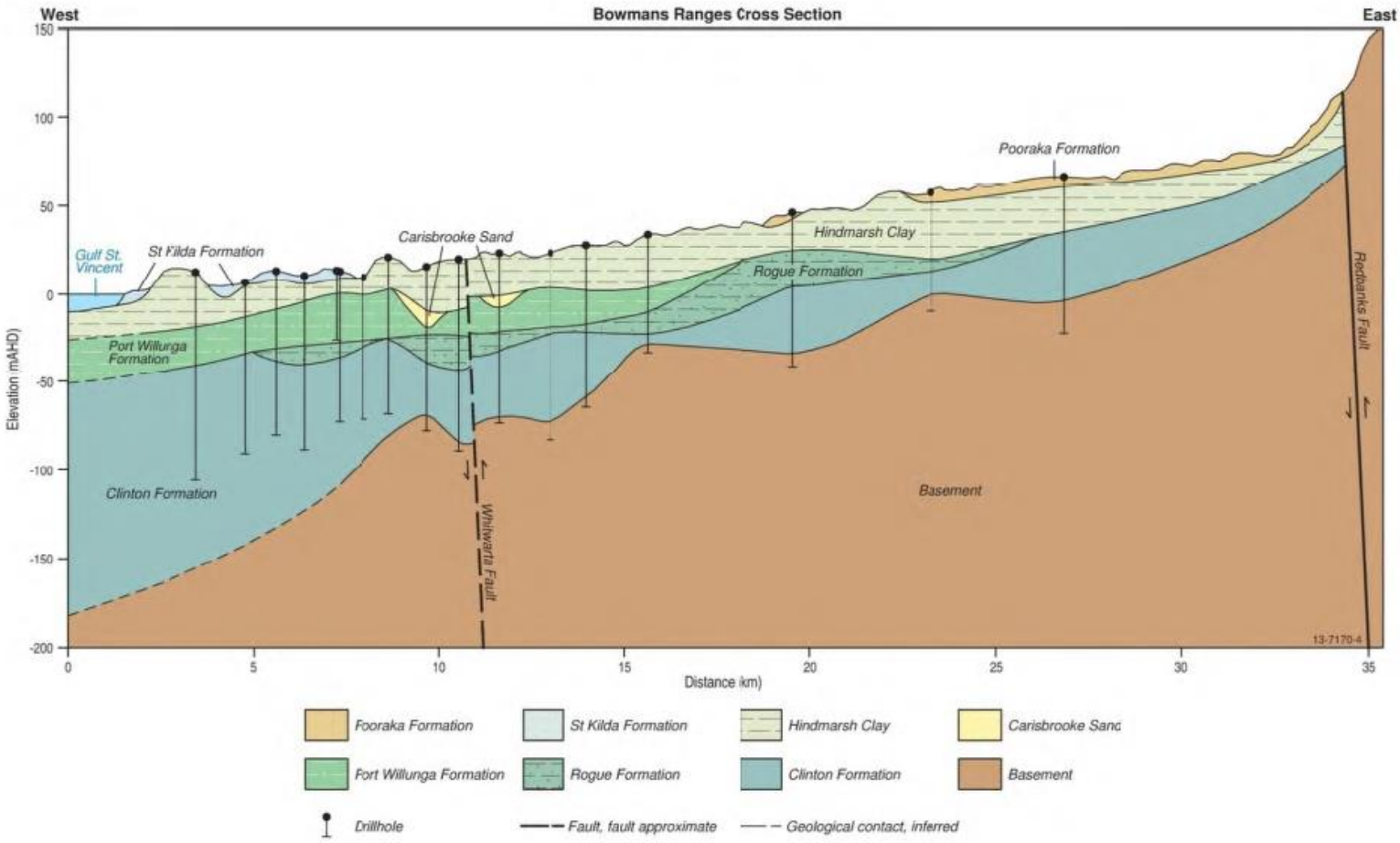

Figure 7. Bowmans to the ranges cross section (Smith *et al*, 2015, licensed under CC BY 4.0).

The drillhole density and depth is significantly lower in the Lower north cross section (Figure 8) than the previous one (Figure 7). However, it still shows a transition from the Port Willunga to the Rogue Formation. Unlike in the Bowmans to the Ranges cross section, the Clinton Formation doesn't extend below the Rogue Formation, yet again, this might be because there weren't drillholes deep enough to reveal the layering accurately.

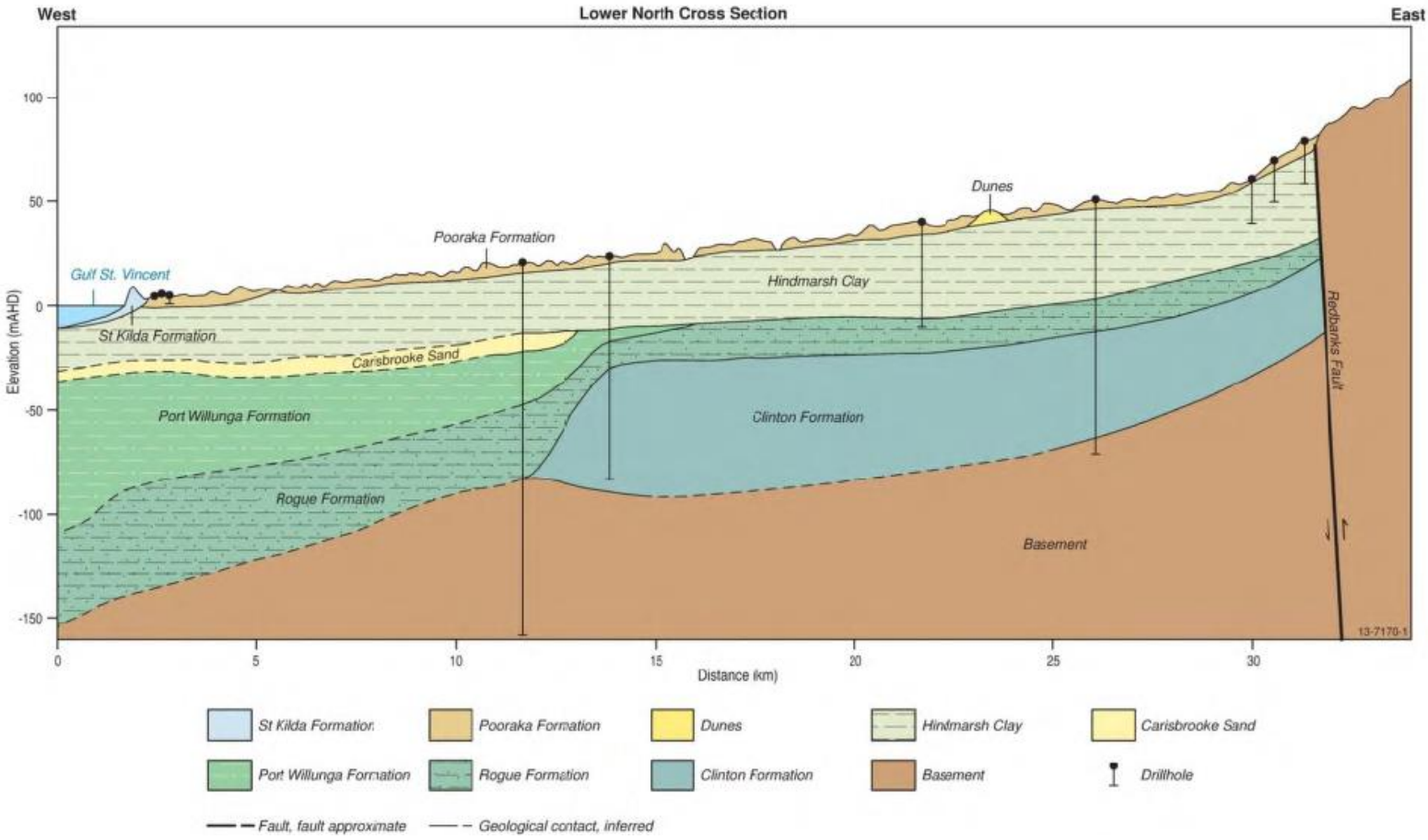

Figure 8. Lower north cross section (Smith *et al*, 2015, licensed under CC BY 4.0).

In Figure 9 it can be seen that the Port Willunga Formation does not extend all the way to the Wakefield River, and the Carisbrooke Sand seems to be discontinuous. The Rogue Formation seems to have a short discontinuation and the Clinton appears to be continuous. It is also worth noting how, overall, the bottom depth and thickness of the Tertiary units decrease as they go north, with the basement taking over.

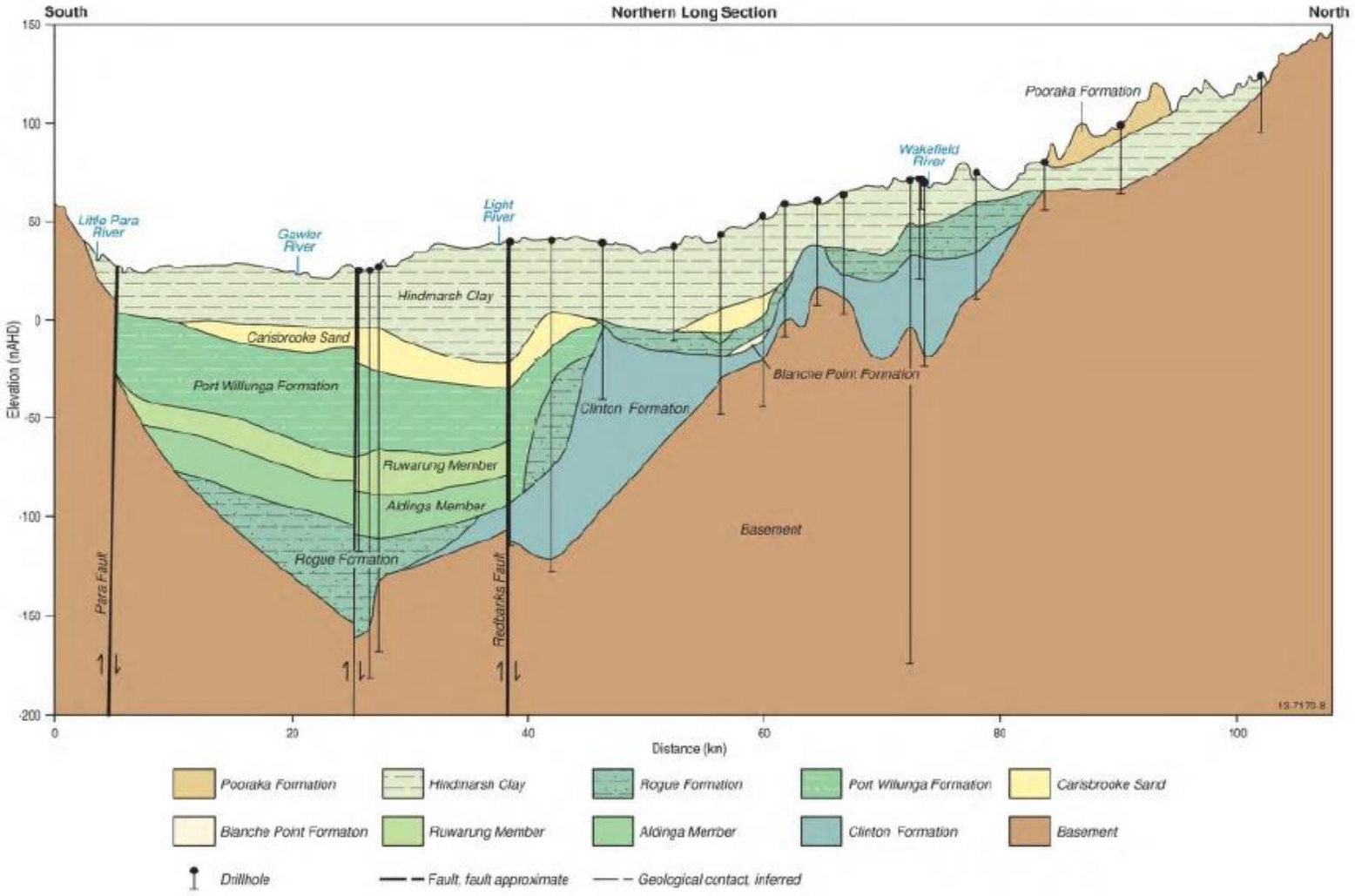

Figure 9. Northern long section cross section. Although this cross section is bigger, it's easy to locate the portion that is within the NAC thanks to the labels of the rivers (the Wakefield and the Light) (Smith *et al*, 2015, licensed under CC BY 4.0).

1.7 Hydrogeological conceptual model

Information regarding the hydrostratigraphy from several sources was analysed, including technical reports, scientific articles, and government databases. With this information, an initial hydrogeological conceptual model was elaborated (Figure 10). There are four main hydrogeological layers in the NAC: the Quaternary unit, Port Willunga Formation, Rogue Formation, and the Clinton Formation. The aquifer denomination adopted for this study is the one from the WaterConnect database: Q1–Q3 for Quaternary aquifers, Qpac for the Carisbrooke Sand, T1 for the Port Willunga Formation, Teor for the Rogue Formation, and Teoc for the Clinton Formation.

The Quaternary unit comprises the Hindmarsh Clay and the Carisbrooke Sand, and it's the topmost layer of the study area. It's mainly composed of clay, and in a lesser degree, sand. There are four aquifers in the Quaternary unit: Q1, Q2, Q3 and Q4 or Qpac. Q1–Q3 aquifers are unconfined, discontinuous and occur mainly in sandy intervals interbedded within the Hindmarsh Clay. The Qpac

is a confined aquifer that occurs only in the Carisbrooke Sand (Smith *et al*, 2015). It's larger than the Q1–Q3 and it might have hydraulic connection with the Tertiary aquifers, especially if it's not underlain by the Hindmarsh Clay. Recharge to the Q1–Q3 aquifers is expected to be from the seasonal rainfall and river leakage from the Light and Wakefield Rivers mainly. Groundwater extraction is mainly for stock and domestic, centred on the towns, with no estimates on extraction provided, but expected to be low since there's almost no irrigation agriculture. Evapotranspiration is potentially quite high, especially for the unconfined aquifers (Smith *et al*, 2015). Bresciani *et al* (2018) reported a median value of 1300 mg/L of salinity for the Quaternary aquifers in the NAP and Central Adelaide Plains (CAP).

The Port Willunga Formation underlies the Quaternary unit and is mainly composed of limestone. It's confined and is believed to be the highest yielding aquifer in the study area. It might be in hydraulic connection to the Carisbrooke Sand and Rogue Formation. The range of horizontal hydraulic conductivity (K_H) reported for the T1 limestone aquifer in the NAP goes from 0.63 to 120 m/d (Bresciani *et al*, 2015a; Bresciani *et al*, 2015b). The K_H values of the limestone aquifer in the NAC are expected to be around that range. According to a map reported by the Goyder Institute for Water Research (2016), the salinity values of the limestone aquifer in the NAC range from 2,000 to 14,000 mg/L.

Little is known about the hydrogeological characteristics of the Rogue and Clinton Formations since they aren't present in the NAP. It's possible that these two formations are hydraulicly connected. The general groundwater flow is believed to go from east to west, discharging to the sea. Groundwater may also flow south from the NAC to the NAP, but this hasn't been determined.

Regarding the recharge to the confined aquifers in the study area (Qpac, T1, and possibly Teor and Teoc) is expected to come from both the Mountain Front and Mountain Block as some studies (Batlle-Aguilar *et al* 2017 and Bresciani *et al* 2018) have discussed for the aquifers in the NAP, although it is unknow which mechanism is the predominant one in the NAC.

Figure 10 depicts the hydrogeological conceptual model of the NAC in which the stratigraphy, relevant geographical features and the main (expected) groundwater flows are shown. It is expected that the water table in the unconfined aquifers resembles the topography, being higher in the Mount Lofty Ranges and decreasing as it goes west, driving the flow towards the sea. As shown in Figure 4, the Mount Lofty Ranges receive more rainfall than the rest of the region, adding to the probability of it being the main area for groundwater recharge.

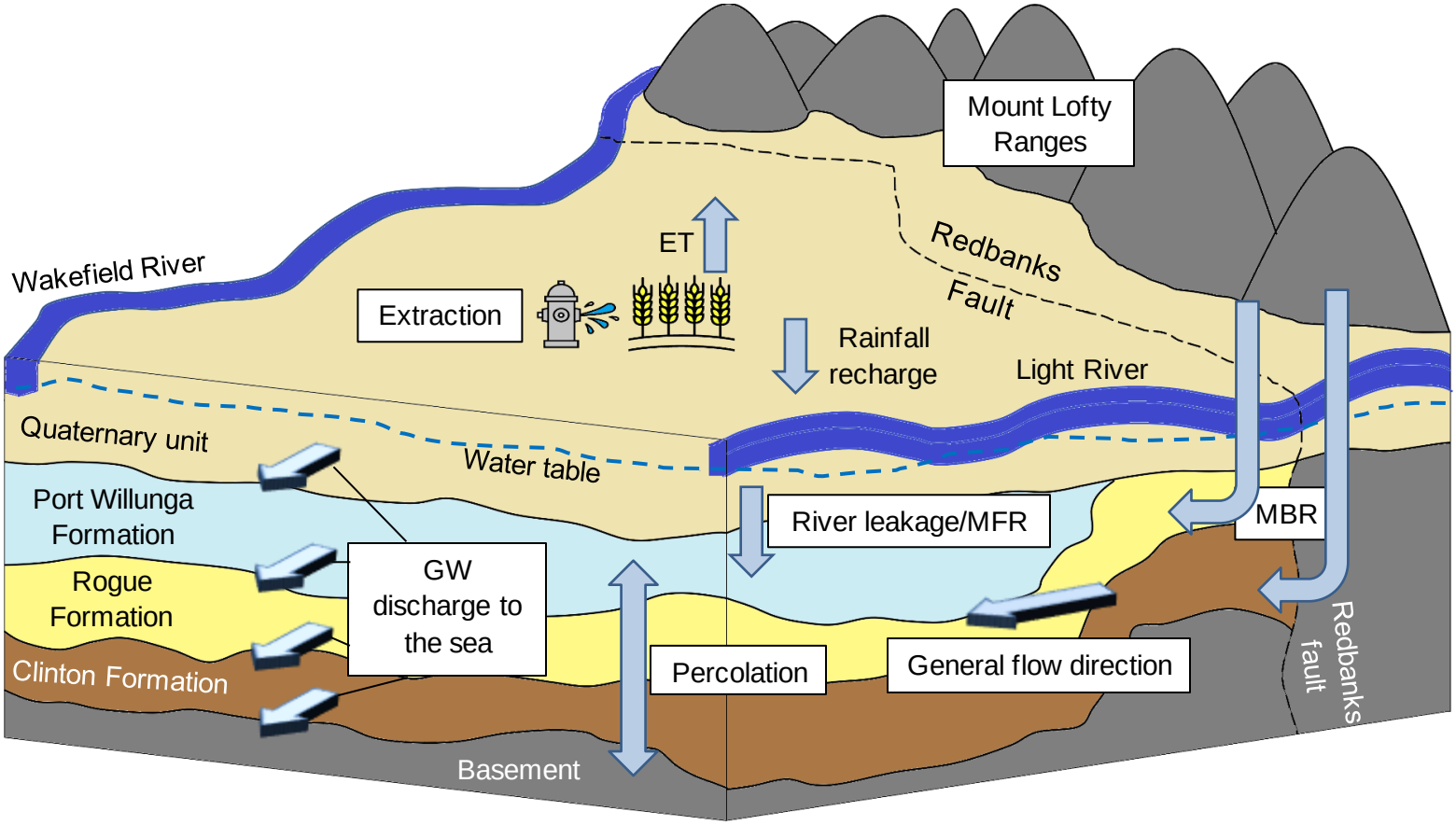

Figure 10. Hydrogeological conceptual model of the Northern Adelaide Corridor. Note how the RF and CF don't extend past the Redbanks Fault. The double ended arrow means groundwater can flow either way.

1.8 Creation of continuous stratigraphic layers

The process started by retrieving records of all the wells (or boreholes) with lithological, driller's, stratigraphic and hydrostratigraphic logs, present in the study area and within a 5 km buffer, from the WaterConnect database. As a result, records of over 800 wells were obtained including water, mineral, engineering, and petroleum wells. These records can be lumped into two main types based on the type of information they contain: lithological and stratigraphic.

The lithological logs, just like the name implies, registers the lithology encountered as the bore was drilled, recording the depth at which each lithology was found, and most of the time they provide a brief description of it. The driller's logs present this type of information as well. The lithological logs usually don't contain information about the hydrogeological units encountered in the drillhole. The other type of log is the stratigraphic (and hydrostratigraphic), that only contains the depth at which the hydrogeological units end. This type of logs doesn't provide information about the type or variations in lithology within a hydrogeological unit. Some wells have both a lithological and a stratigraphic type of log, making easier the interpretation and matching of the lithologies to their hydrogeological units. However, most of the boreholes have only one type of log.

The stratigraphic and lithological information of each well was sorted and curated to identify the depth at which each of the main hydrogeological layers end. 493 wells resulted to have enough information to determine at least the depth of one hydrogeological layer. Of these 493 boreholes, 161 have only lithological logs, 322 have only stratigraphic logs and 10 have both.

Table 1 shows the occurrence of each layer in the logs (end depth, except for the basement, for this one is start depth). As expected, the layer with more records is the Quaternary unit since is the topmost. On the other hand, the layer with the least records is the Port Willunga since it's only present in the west and southwest part of the NAC. Note that the total well count in Table 1 adds more than 493 because one well log can provide information of more than one layer.

Table 1. Number of wells with end depth per layer.

Layer	Well count
Quaternary unit	420
Port Willunga Formation	71
Rogue Formation	179
Clinton Formation	136
Basement	268

The boreholes aren't evenly distributed throughout the study area, there are some portions of it where the density of drillholes is low generating uncertainty. Figure 11a shows the distribution of wells with end depth of at least one hydrogeological layer in the study area and the type of log they contain. Figures 11b to 11f show the borehole distribution per hydrogeological layer.

The biggest gaps can be appreciated in Figure 11a in the middle-west portion of the study area, zones of around 50 km^2 without a log. The Quaternary logs are well distributed throughout the study area (see Figure 11b). The Port Willunga, Rogue and Clinton Formations, and the basement present major gaps in the south and south-west portion of the study area (Figures 11c to 11f). This is because most of the wells here end shortly after tapping into the Port Willunga Formation (according to the logs) since it's presumably the highest yielding aquifer in the study area. As a result, not a lot of wells reach the end of the Port Willunga Formation making the stratigraphy quite uncertain. From the few wells that reach the end of the Port Willunga Formation, it is known that this layer thickens in that portion of the study area, exceeding the 100 m thickness even.

It is also worth noting that none of the Tertiary units (Port Willunga, Rogue and Clinton Formations) are found in any log east of the Redbanks Fault, being consistent with the cross sections of Figures 7 and 8.

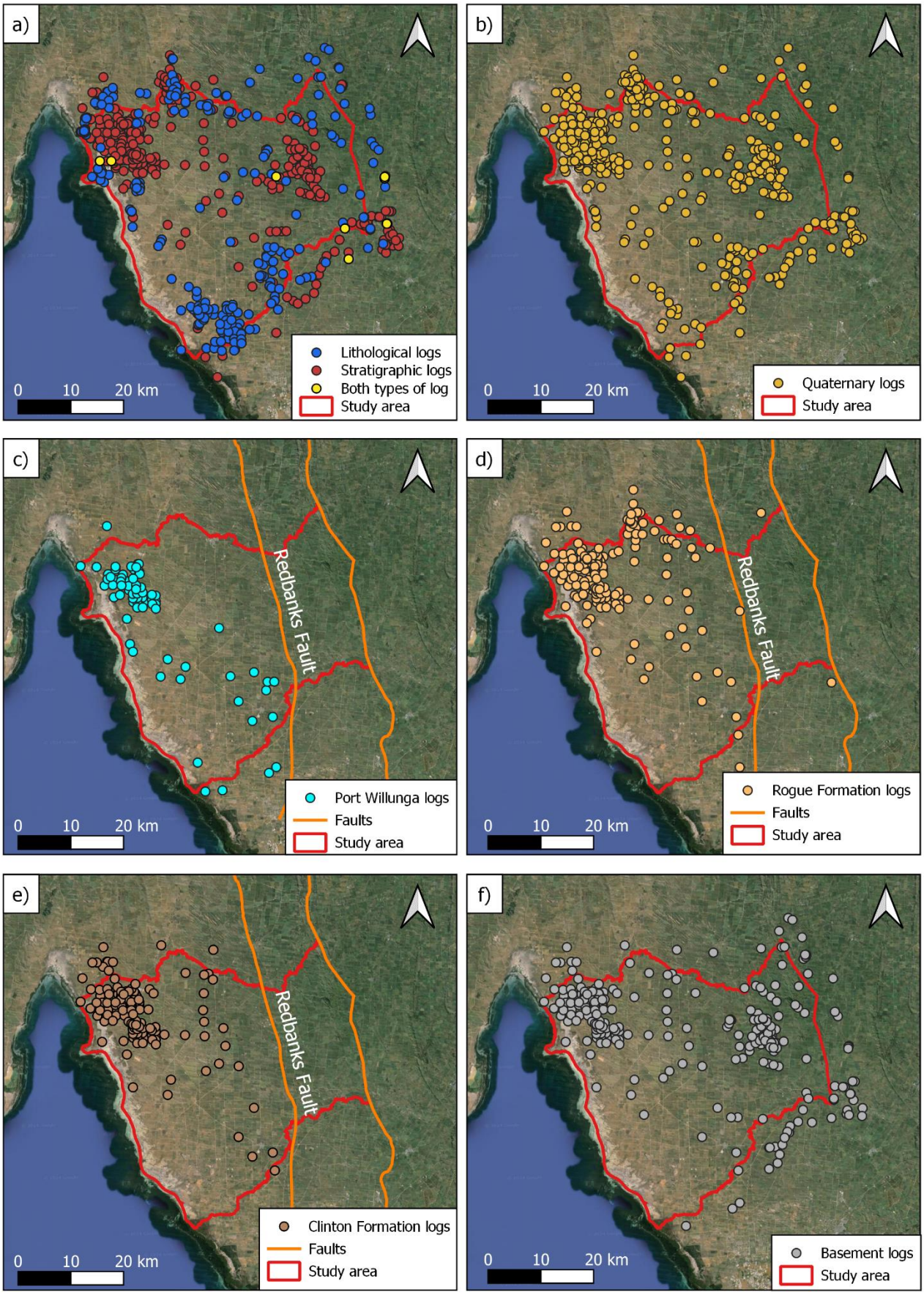

Figure 11. Spatial distribution of wells in the study area: a) types of logs; b) logs; c) Port Willunga logs; d) Rogue Formation logs; e) Clinton Formation logs; f) basement logs.

The depth information of each well was converted to m AHD by subtracting the layer end depth to the ground elevation of the well. For the wells that didn't have ground elevation data, it was obtained by reading it from the same DEM mentioned in Section 1.3. Later, the wells were separated into two groups, the ones for interpolation and the ones for validation to test the goodness of fit of different interpolation methods. The size of the validation groups was 20% of the well count per layer, taking care that they were well distributed around the study area to prevent bias. The interpolation methods tested were IDW with powers of 0.5, 1, 2, 3 and 4; ordinary kriging with circular, exponential, gaussian, linear and spherical semivariograms; universal kriging with linear and quadratic drifts; natural neighbour; regularized spline with 0.1 and 0.3 weights; and tension spline with 0.1 and 0.3 weights. The raster layers were created in ArcGIS with a square pixel size of 25 m.

Once all interpolation layers were obtained, they were compared against the validation points by subtracting the interpolated depth value to the log depth value. Then, those results were squared, summed, and then divided by the number of validation points to find the interpolated layer with the lowest Mean Squared Error (MSE) (best fit). Table 2 contains the number of wells for interpolation and validation, and the best interpolation method and MSE per layer.

Table 2. Interpolation and validation data sets per layer. The number next to "IDW" means the power used.

Layer	Number of wells used for interpolation	Number of wells used for validation	Best interpolation and MSE
Quaternary unit	336	84	IDW 1: 176.27
Port Willunga Formation	56	15	Ordinary kriging with gaussian semivariogram: 156.08
Rogue Formation	143	36	IDW 0.5: 89.54
Clinton Formation	108	28	IDW 2:179.64
Basement	214	54	Ordinary kriging with exponential semivariogram: 236.08

The layer with the best fit (lowest MSE) was the Rogue Formation, on the other hand, the one with the highest MSE was the basement. The MSE of the Quaternary unit, Port Willunga and Clinton Formation was similar. These rasters are the foundation for the MODFLOW model layers.

1.9 Fieldwork

Another research project conducted fieldwork in the NAC, in parallel with the developing of this project. The main contribution of the fieldwork to this project were hydraulic head measurements taken in six bores that hadn't been pumped in many years, to be added to the calibration dataset (see Section 2.4). Also, it was confirmed during the fieldwork that there are permanent pools in the Wakefield and Light Rivers (see Section 2.3.2).

2. NUMERICAL MODEL SETUP

2.1 Modelling extent and discretisation

The modelling extent is identical to the extent of the study area in Figure 2 except for the western boundary. This boundary was extended five kilometres away from the coast (see Figure 12) to account for the coastal boundary condition explained in section 2.3.1 The model domain was discretised into 5 layers with grid cells of 500 m by 500 m, yielding 117 rows and 119 columns. The model was based on MODFLOW-NWT and set to be steady-state with units of m/day.

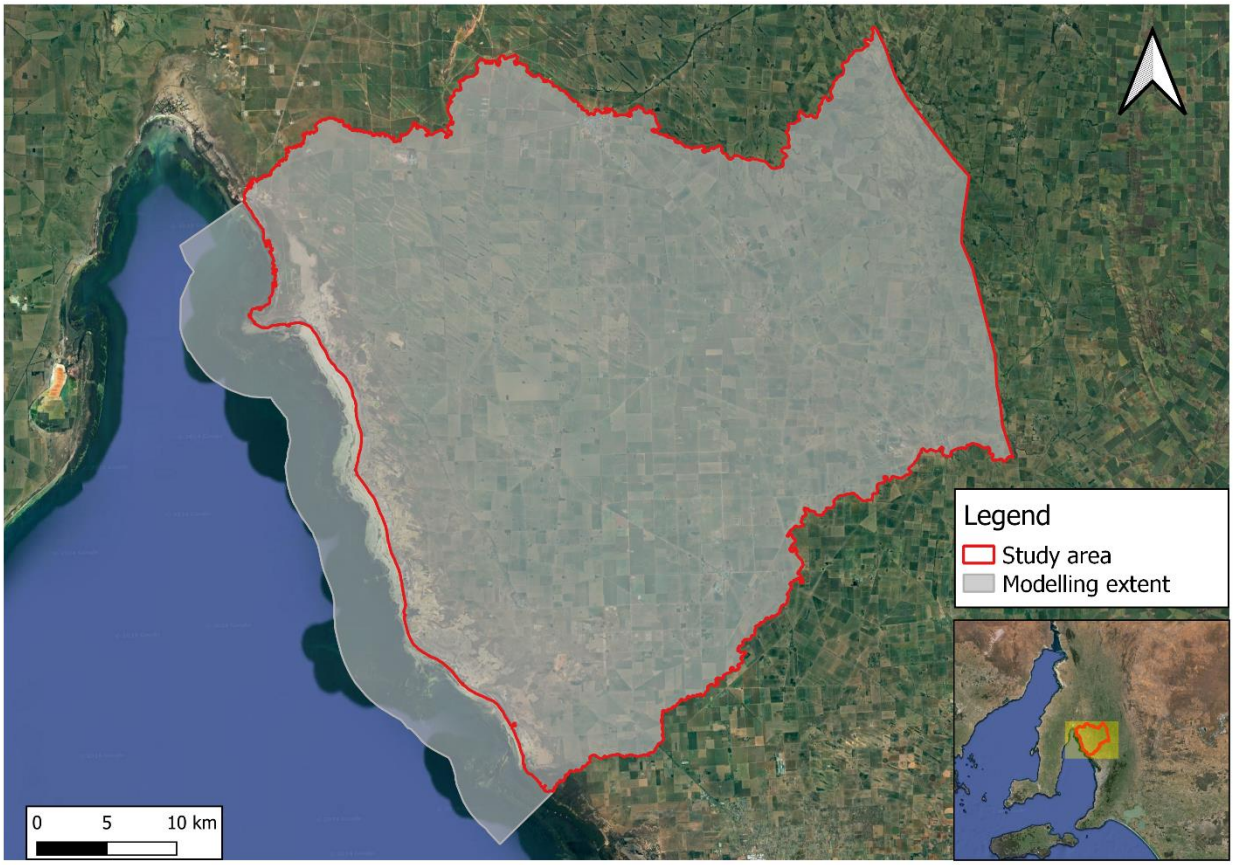

Figure 12. Comparison between the modelling extent and the original study area.

2.2 Layer distribution

2.2.1 Surface elevation (model top)

The model top was set using the DEM shown in Figure 3. Since the grid cell size of the model (500 m x 500 m) is bigger than the pixel size of the DEM (25 m x 25 m), the option selected in ModelMuse was to average all the pixels within a grid cell and assign that value to it (see Figure 13). For the model top which extends five kilometres offshore, a bathymetry dataset published by Geoscience Australia was used. The pixel size of this dataset is 250 m by 250 m.

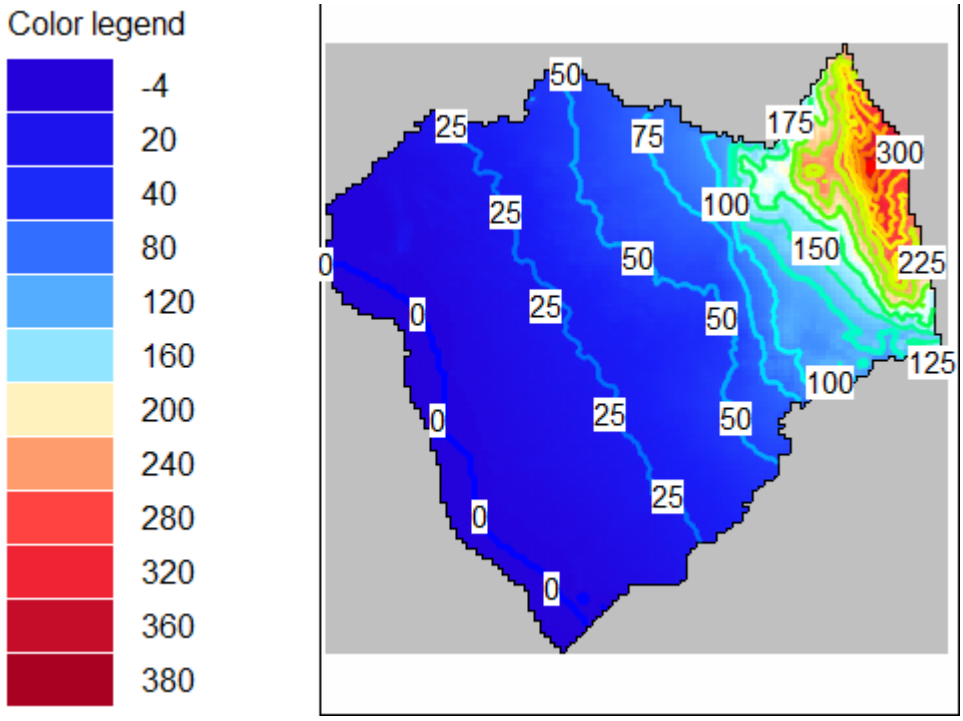

Figure 13. Model top in m AHD.

2.2.2 Layer definition and elevation

The model was divided into 5 layers to represent the main units. Table 3 shows the model layers and the corresponding formations they intersect.

Table 3. Description of the model layers.

Model layer	Hydrostratigraphic unit	Aquifer code or aquitard
1	Hindmarsh Clay	Aquitard
2	Hindmarsh Clay / Carisbrooke Sand	Aquitard / Q4
3	Port Willunga / Rogue / basement	T1 / Teor / aquitard
4	Rogue / basement	Teor / aquitard
5	Clinton / basement	Teoc / aquitard

The elevations of the bottom of the Quaternary unit, Port Willunga, Rogue and Clinton Formations (layers 2, 3, 4 and 5 of the model, respectively) were set with the rasters explained in section 1.8. Unfortunately, these rasters presented conflicts or discrepancies in some small areas in the sense that the bottom of a layer went over the bottom of its overlaying layer (Port Willunga going over the Quaternary for example, or Clinton Formation going over the Rogue Formation). These discrepancies were likely to be caused by the uneven distribution of logs (data gaps, see Figure 11), the interpolation method and the discontinuity of the hydrogeological layers. The latter means that not all the logs show the sequence Quaternary–Port Willunga–Rogue–Clinton–basement (for the wells that tap into the Port Willunga) or the sequence Quaternary–Rogue–Clinton–basement (for the ones that don't). Some logs "skip" one or more layers meaning that that layer is not present in that

spot. However, for the simplicity of the model, it was assumed that, west of the Redbanks Fault, the Tertiary units extend continuously across the modelling extent except the Port Willunga Formation. For this layer, a polygon was drawn to approximate its extent based on the logs that tap into it (Figure 14c). Figure 14 shows the extent of the hydrostratigraphic units per layer of the model.

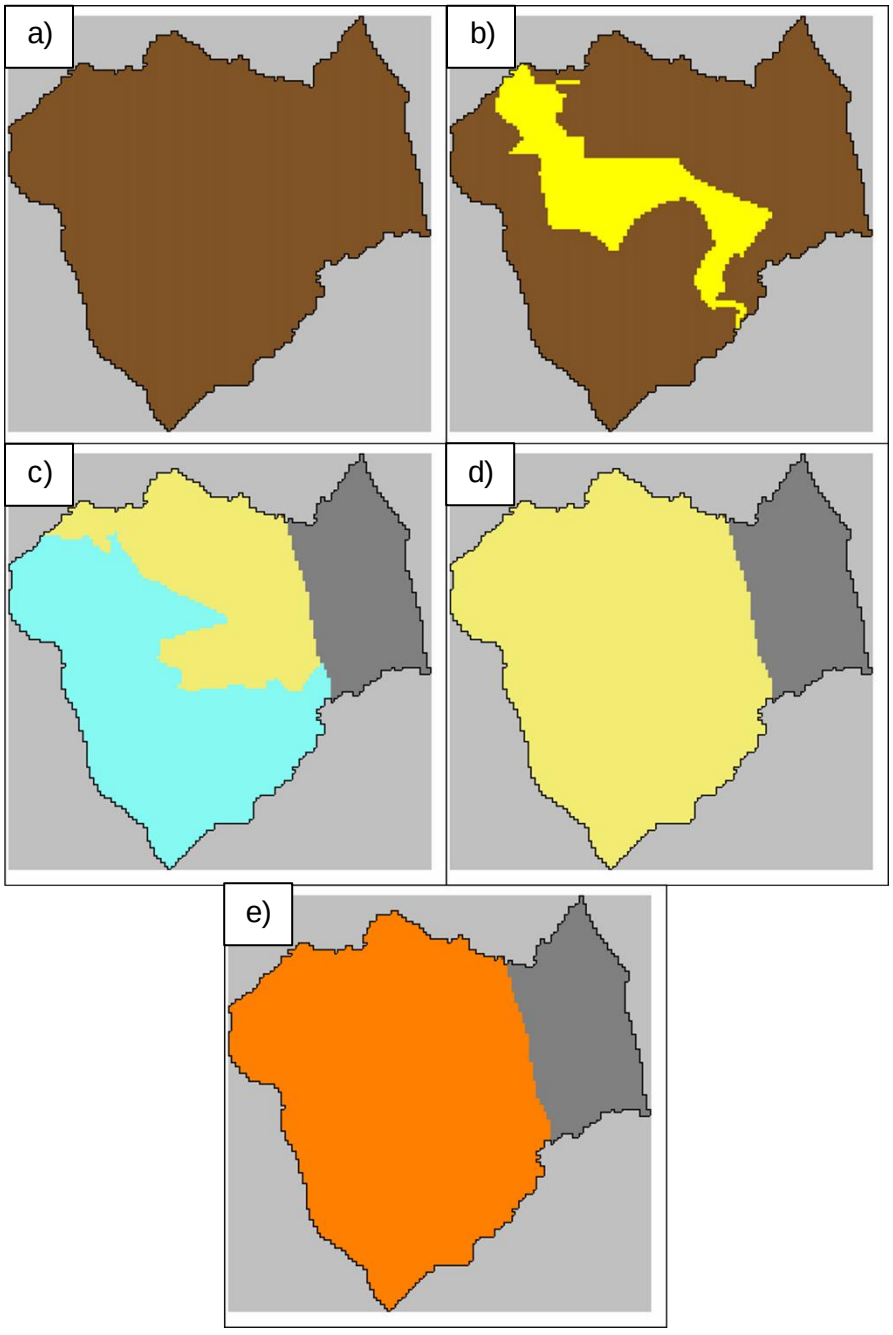

Figure 14. Horizontal extent of the hydrostratigraphic units: a) layer 1: Hindmarsh Clay; b) layer 2: Hindmarsh Clay (brown) and Carisbrooke Sand (yellow); c) layer 3: Port Willunga Formation (light blue), Rogue Formation (beige) and basement (grey); d) layer 4: Rogue Formation (beige) and basement (grey); e) Clinton Formation (orange) and basement (grey).

The discrepancies mentioned earlier were manually corrected in ModelMuse by creating polygon objects where the discrepancies were and assigning an elevation value to those objects based on the nearest(s) log(s) (an average of the elevations if more than one log was useful) for the layers in question. Figures 15 to 18 show the model's bottom elevations of the Quaternary, Port Willunga, Rogue and Clinton Formations (layers 2 to 5, respectively).

The Quaternary bottom (Figure 15), as expected, resembles closely the surface elevation (Figure 13).

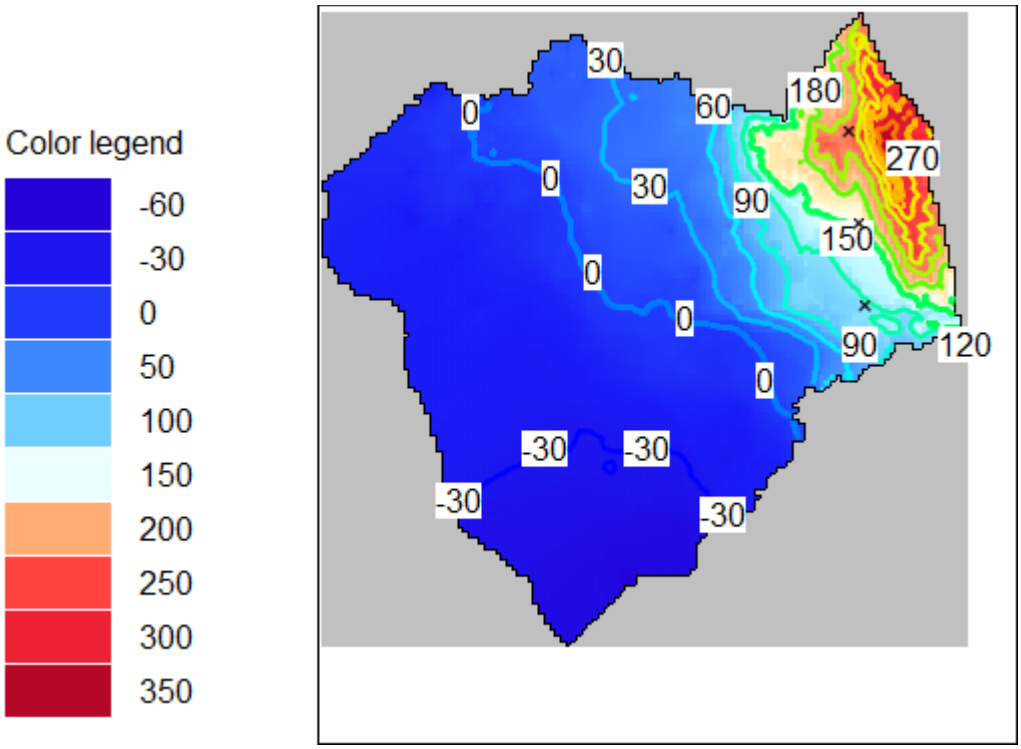

Figure 15. Quaternary bottom in m AHD.

The bottom of the Port Willunga Formation in Figure 16 corresponds to the area in blue only (see Figure 14 for the extent of this formation). Since it isn't possible to create discontinuous layers in ModelMuse, the bottom of the rest of the area displayed in Figure 16 (white and red portions of the figure) was set to be half the depth between the bottom of the Quaternary and the bottom of the Rogue Formation (see Figure 17). Note that the colors don't extend past the Redbanks Fault.

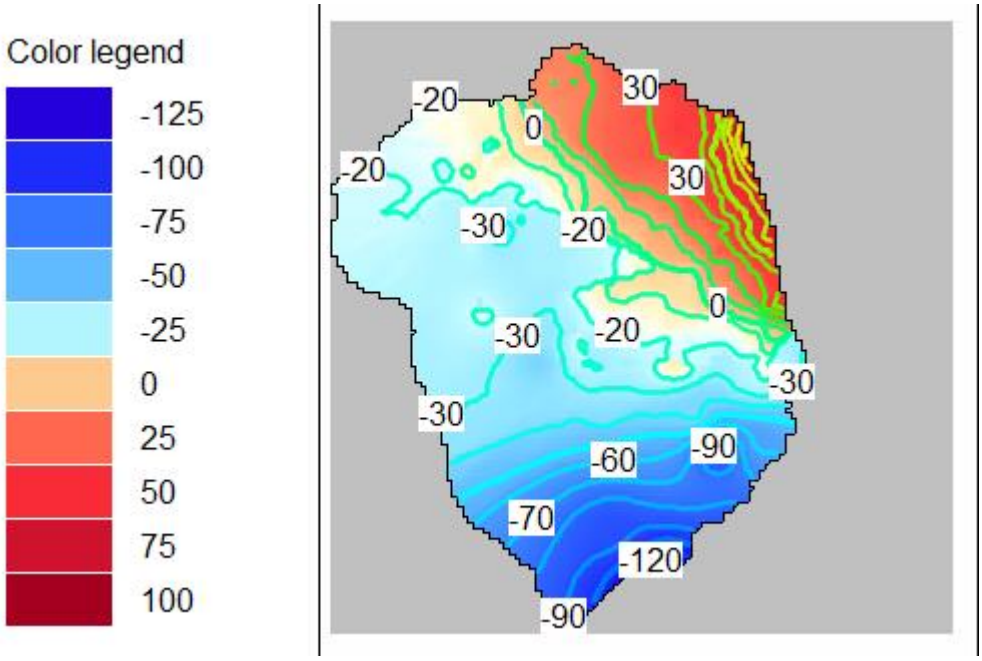

Figure 16. Port Willunga Formation bottom in m AHD.

Figure 17 shows the actual Rogue Formation bottom everywhere in the figure. Note that the colors don't extend past the Redbanks Fault.

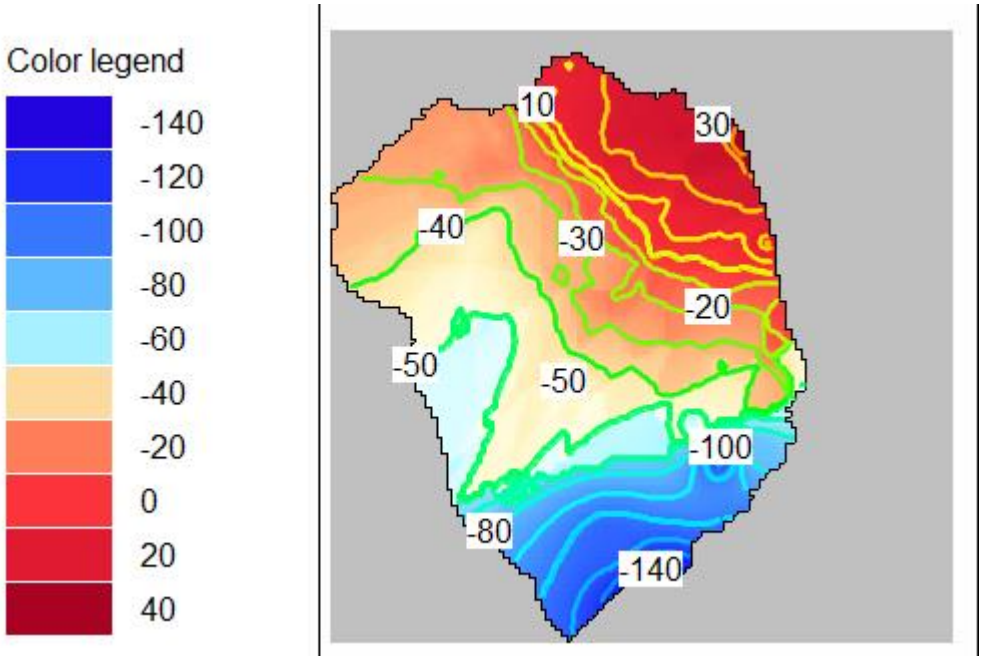

Figure 17. Rogue Formation bottom in m AHD.

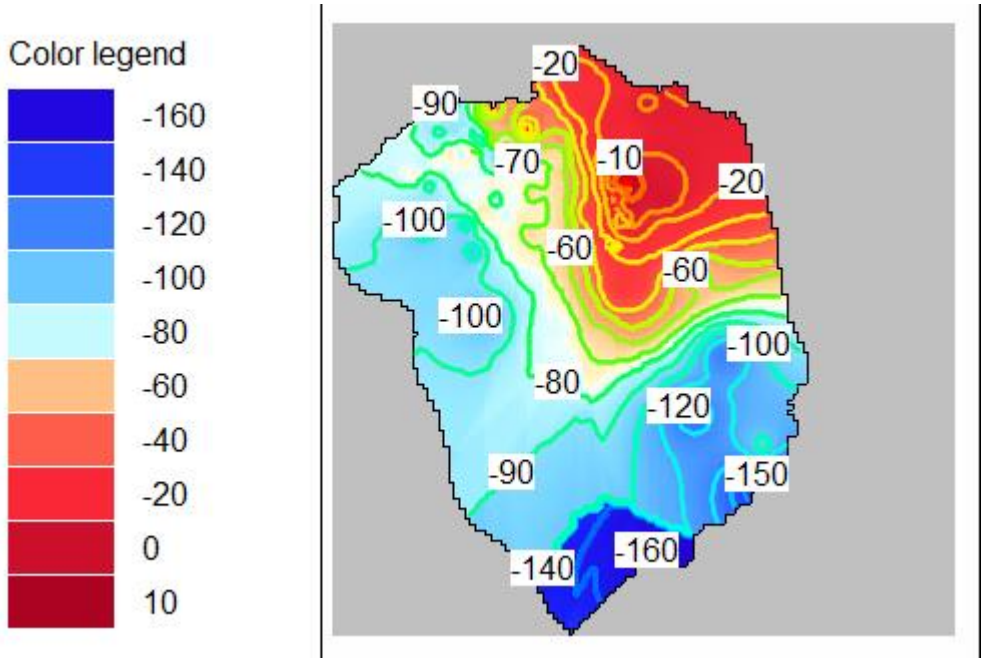

Figure 18. Clinton Formation bottom in m AHD.

The numerical model has a vertical extent or range of 546 m, being the highest point 382 m AHD in the Mount Lofty Ranges and the lowest point -164 m AHD in the Clinton Formation bottom.

An attempt was made to determine the location and extent of the sandy aquifers in the Quaternary unit (Q1 to Q4) by matching the information of the lithological logs for several drillholes. The sand lenses present in the lithological logs were sorted by start and end depth, and thickness. Then polygons were drawn guided by the bores with similar sand lenses and that were close to one another. As a result, seven polygons were drawn approximating the extent of the sand lenses: three for the Q1, one for the Q2, two for the Q3, and one for the Carisbrooke Sand (Q4). Figure 19 shows the approximated sandy aquifer polygons and the boreholes that present sand lenses in their logs.

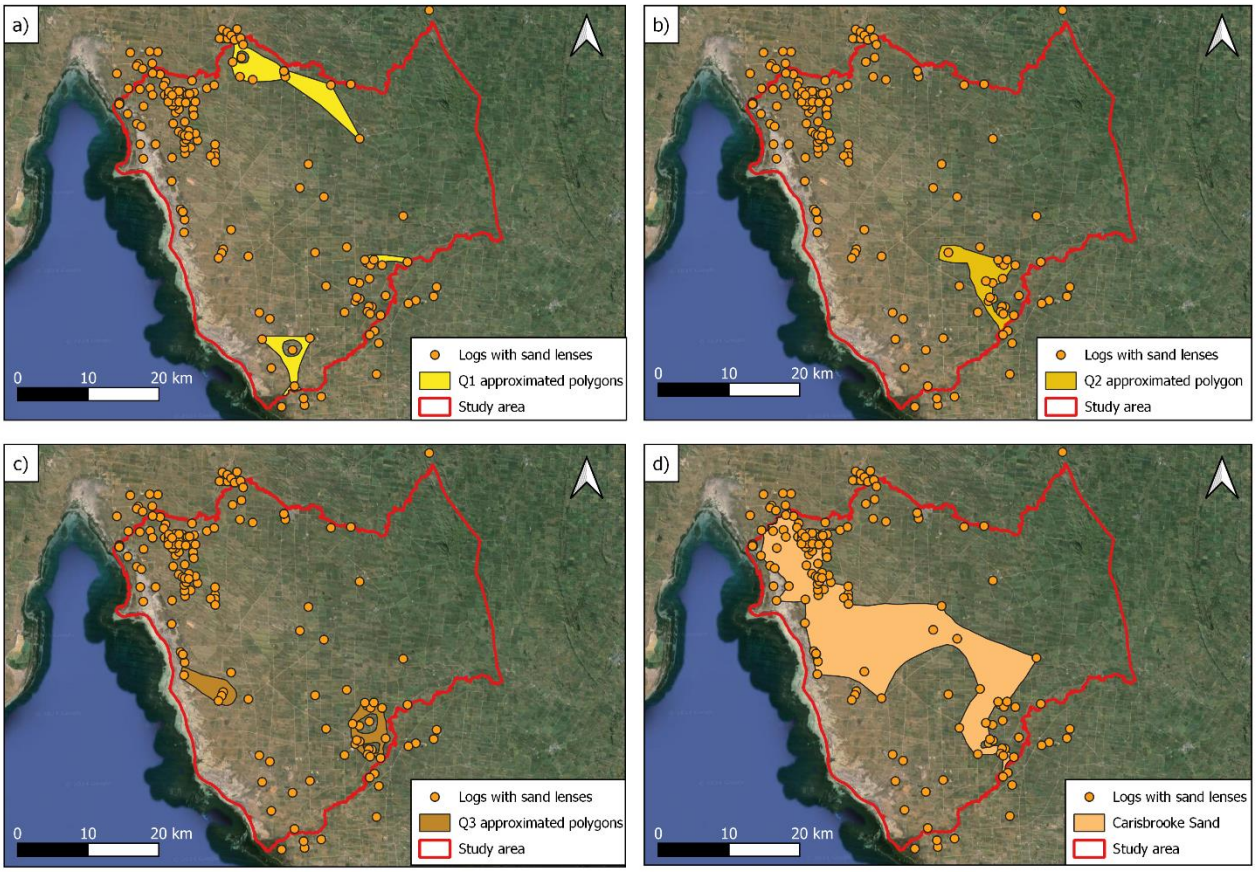

Figure 19: a) Approximated extent of the Q1; b) Q2; c) Q3; and d) Carisbrooke Sand (Q4) sandy aquifers.

Some of the sand lenses have an odd appearance, these shapes are unlikely to occur in reality. Because of this, only the Carisbrooke Sand polygon was imported to ModelMuse. The elevations of the start and end of the Q4 aquifer were determined averaging the values reported in the logs that were used to draw their extent.

2.2.3 Layers' hydraulic properties

The initial value of horizontal hydraulic conductivity (K_H) for each layer is shown in Table 4. The K_H value used for the Hindmarsh Clay and the basement are the same as the initial values used by Bresciani *et al* (2015a), and the K_H assigned to the Port Willunga Formation was the calibrated value for T1 reported by the aforementioned authors. For the rest of the layers, arbitrary values close to the median of the ranges reported by Fitts (2013) (chapter 3, figure 3.2) were used according to their dominant geologic material. The Clinton Formation K_H is one order of magnitude less than the Q4 aquifer, despite the fact that both are mainly composed of sand, because the former contains lignite, silt, and clay. The vertical hydraulic conductivity (K_V) was let to be a tenth of the K_H.

Table 4. Initial values of K_H.

Hydrostratigraphic unit	Dominant geologic material	Initial K_H (m/day)	Initial K_V (m/day)
Hindmarsh Clay	Clay	$3.1x10^{-3}$	$3.1x10^{-4}$
Carisbrooke Sand (Q4)	Sand	5	0.5
Port Willunga Formation (T1)	Limestone	0.63	0.063
Rogue Formation (Teor)	Sandstone	0.05	0.005
Clinton Formation (Teoc)	Sand	0.5	0.05
Basement	Different types of rocks (fractured)	0.001	$1x10^{-4}$

Figure 20 shows six cross sections of the model to assist with the visualization of the layering. The colours are the same as for Figure 14.

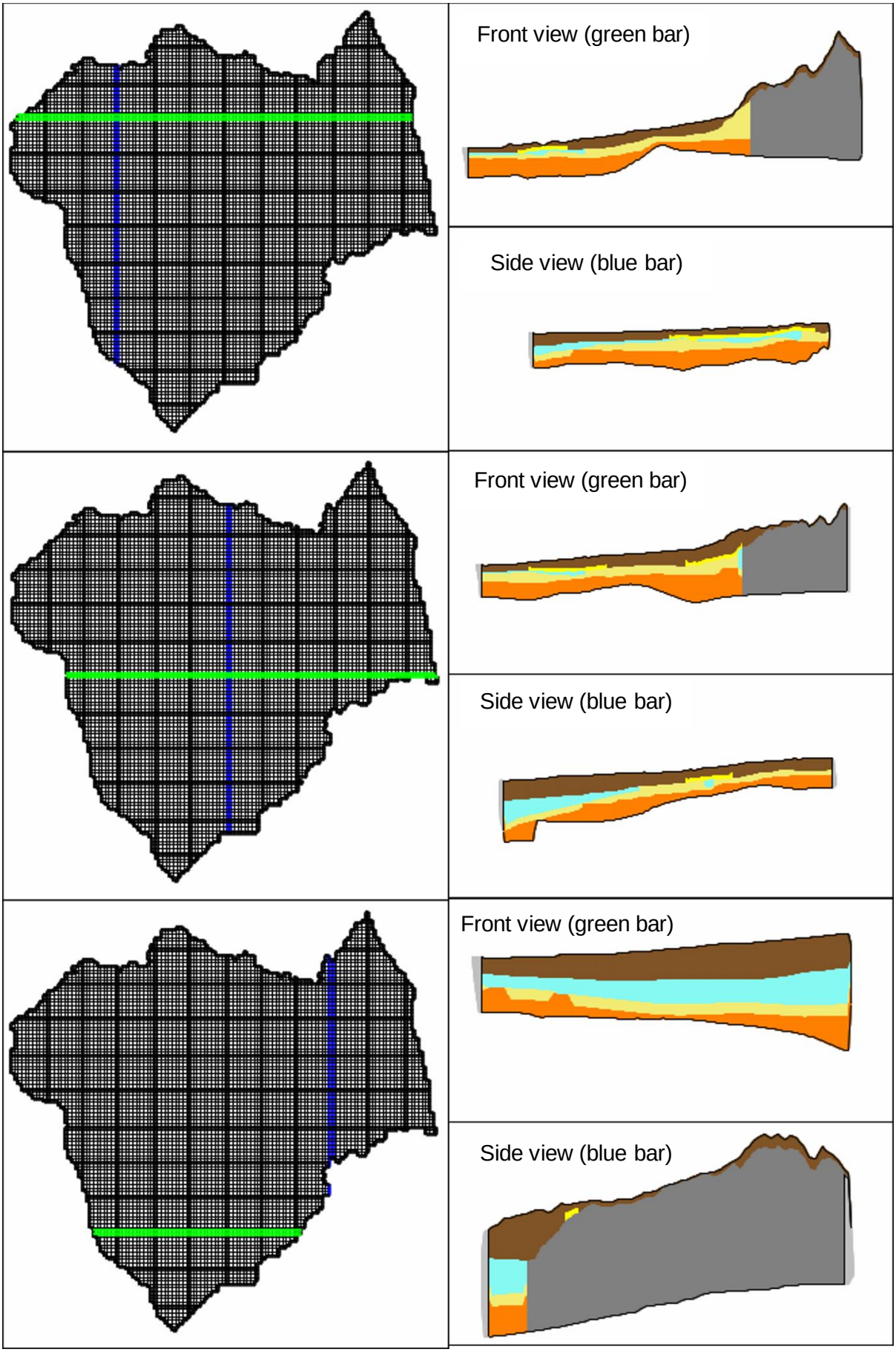

Figure 20. Cross sections displaying the distribution of the hydrostratigraphic units: Hindmarsh Clay in brown, Carisbrooke Sand in yellow, Port Willunga Formation in light blue, Rogue Formation in beige, Clinton Formation in orange and the basement in grey.

2.3 Boundary conditions

Initially, four boundary conditions were considered for the model: the Alma Fault (eastern boundary), the coastal boundary, the rivers, and the recharge. However, it wasn't possible to specify a general head boundary at the Alma Fault given the lack of hydraulic head data (see section 2.4), and for simplicity, it was just set to be a no flow boundary. The other three boundary conditions were included and are explained in the following sections.

2.3.1 Coastal boundary

This boundary condition extends 5 km offshore and was assigned a constant, equivalent freshwater head of the mean sea level (0 m AHD) with the formula (Guo *et al.* 2002):

$$h_f = \frac{\rho_s}{\rho_f} h - \frac{\rho_s - \rho_f}{\rho_f} Z \qquad \text{Equation 1}$$

where h_f (m AHD) is the equivalent freshwater head, ρ_s and ρ_f (kg/L) are the densities of seawater (1,025 kg/m^3) and freshwater (1,000 kg/m^3) respectively, h (m AHD) is the seawater head (i.e., 0 m AHD) and Z (m AHD) is the elevation at which the equivalent freshwater head is calculated. Z was obtained from the bathymetry of the seafloor. This boundary condition was assigned to all five layers of the model to allow them to discharge to the sea.

2.3.2 Rivers

River flow characteristics of 15 stream gauges (gauging stations) within the study area, from the Water Data SA portal were retrieved and analysed. There are ten gauging stations on the Wakefield River, four on the Light River and one on the Gilbert River, which is a tributary of the Light River. Table 5 summarizes the relevant information of the stream gauges in the study area. The first limitation encountered with this information were the data gaps: only seven stations are currently active (three for the Wakefield River, the Gilbert River one, and three for the Light River) and the data between the active and inactive stations doesn't match each other in time (recordings happened at different times). Furthermore, some of the data of both active and inactive stations, is of very low data quality because the water level was below the minimum recordable value.

Table 5. Relevant information of the gauging stations.

Stream gauge	River	Gauge status	Interval of years with data	Data recorded	Minimum recordable value (m)	River condition
Wakefield River near Rhynie (WR1)	Wakefield	Active	1941-2024	Discharge, EC and water level	0.840	Perennial

Wakefield River upstream the Rocks (WR2)		Inactive	2002-2010	Water level	0.900	Seasonal
Wakefield River 400 m downstream the Rocks entrance (WR3)		Inactive	2001-2010	Water level	0.900	Seasonal
Wakefield River 2 km downstream the Rocks (WR4)		Inactive	2002-2010	Water level	0.900	Unknown: water level below recordable range
Wakefield River 8 km upstream Balaklava (WR5)		Inactive	2002-2009	Water level	0.900	Unknown: water level below recordable range
Wakefield River upstream Balaklava (WR6)		Active	2019-2024	Discharge and water level	1.070	Unknown: water level below recordable range
Wakefield River at Balaklava (WR7)		Inactive	2002-2009	Water level	0.900	Unknown: water level below recordable range
Wakefield River at Whitwarta (WR8)		Inactive	2002-2010	Water level	Couldn't be determined from the data	Perennial
Wakefield River at Port Wakefield (WR9)		Inactive	2002-2009	Water level	0.900	Unknown: water level below recordable range
Wakefield River at Port Wakefield Road (WR10)		Active	2019-2024	Discharge and water level	1.100	Unknown: water level below recordable range
Gilbert River at Stockport (GR1)	Gilbert	Active	2019-2024	Discharge and water level	1.110	Unknown: water level below recordable range

Light River at Hamley Bridge (LR1)	Light	Active	2019-2024	Discharge and water level	0.130	Seasonal
Light River downstream Hamley Bridge (LR2)		Active	2019-2024	Discharge and water level	0.265	Seasonal
Light River upstream school road (LR3)		Active	2019-2024	Discharge and water level	0.035	Dry
Light River at Port Wakefield Rd Bridge (LR4)		Inactive	2010-2017	Discharge and water level	0.000	Seasonal

The spatial distribution of the stations isn't optimal either, Figure 21 shows the location of the stream gauges in the study area. The stations of the Wakefield River have a better coverage than the ones in the Light River.

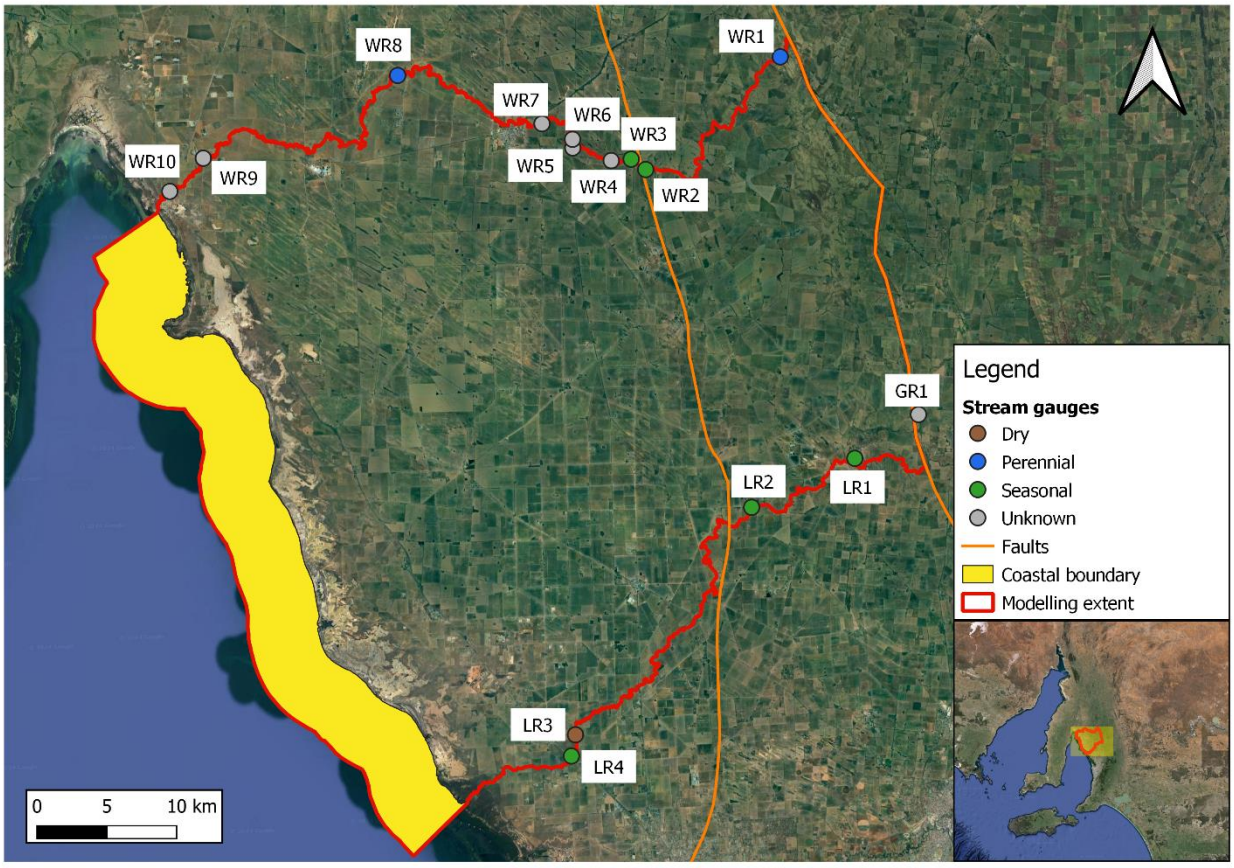

Figure 21. Coastal boundary and location of the stream gauges.

Looking closer at the data, it was found that the upstream stations had more water level recordings (the water level being above the minimum recording value) than the ones downstream, for both

rivers. More specifically, the gauges east of the Redbanks Fault are the ones with more water level recordings. This suggests that the rivers are perennial (gaining streams) and they change to be losing streams after they go past the Redbanks Fault. This phenomenon is also mentioned in the Wakefield River Catchment Action Plan where it reads: "From downstream of the Rocks Reserve to Balaklava a significant portion of flow disappears into sand and gravel beds". The hydrographs of the stations in question are shown in Figures 22-25, they were obtained directly from the Water Data SA page, licensed under CC BY 4.0. There are two bars above the horizontal axis of each graph related to the quality control: grade and approval. For the grade bar the colour blue means "good", green is "fair", yellow is "poor", orange is "water level below recordable range", black is "unverified telemetry". The green colour in the approval bar means "approved" and the red means "working".

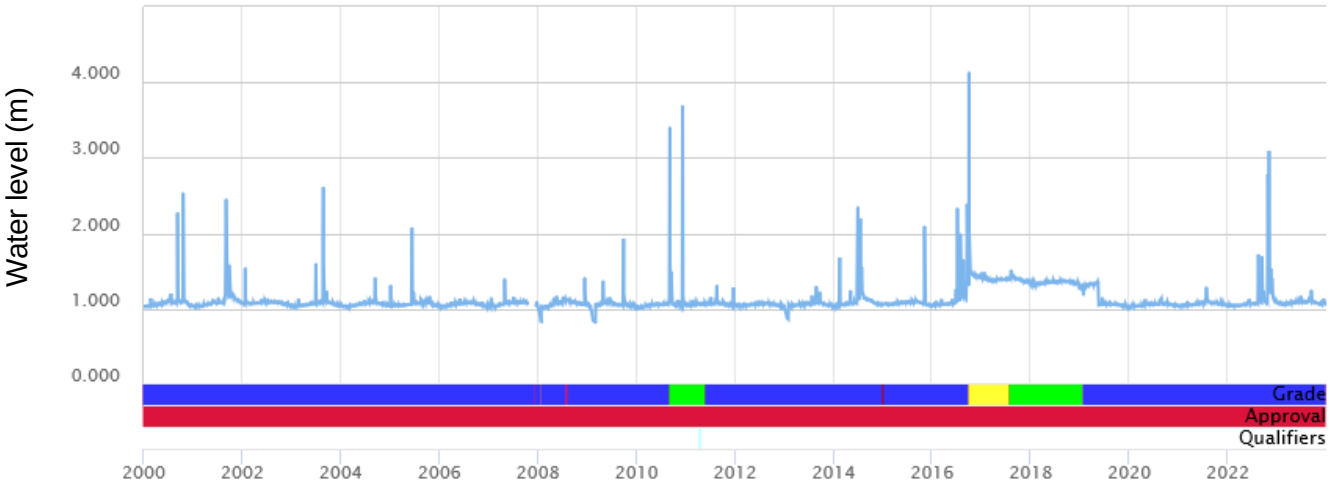

Figure 22. "Wakefield River near Rhynie" (WR1) station hydrograph. Minimum recordable value: 0.840 m

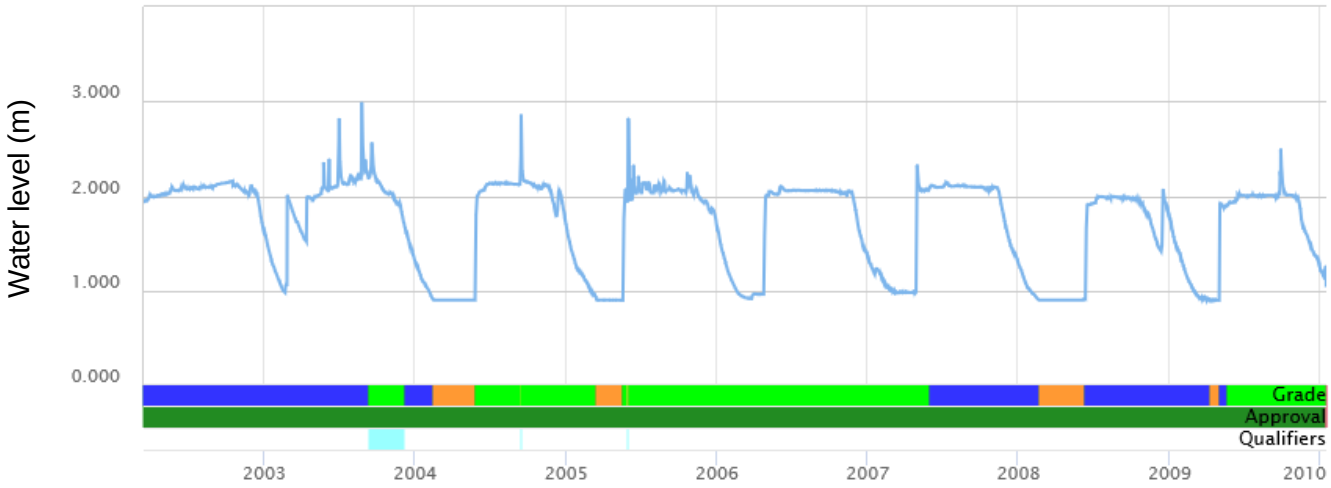

Figure 23. "Wakefield River upstream the Rocks" (WR2) station hydrograph. Minimum recordable value: 0.900 m. This is the closest upstream station to the Rocks Reserve. The stations downstream from this one show a significant decline in water level recordings.

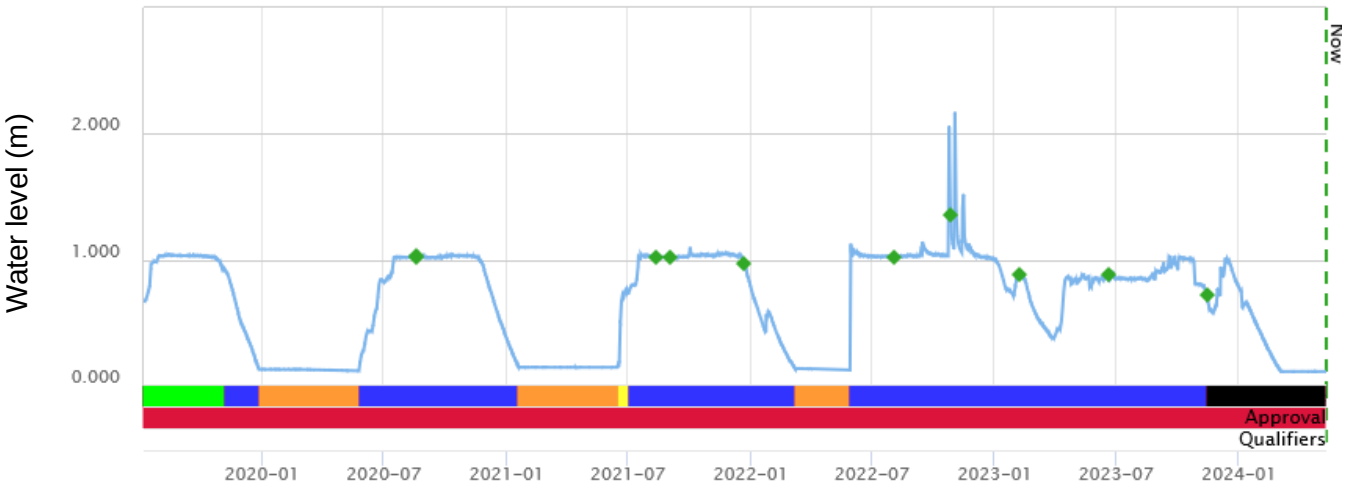

Figure 24. "Light River at Hamley Bridge" (LR1) station hydrograph. Minimum recordable value: 0.130 m. The green rhombuses represent the water level observed during field visits.

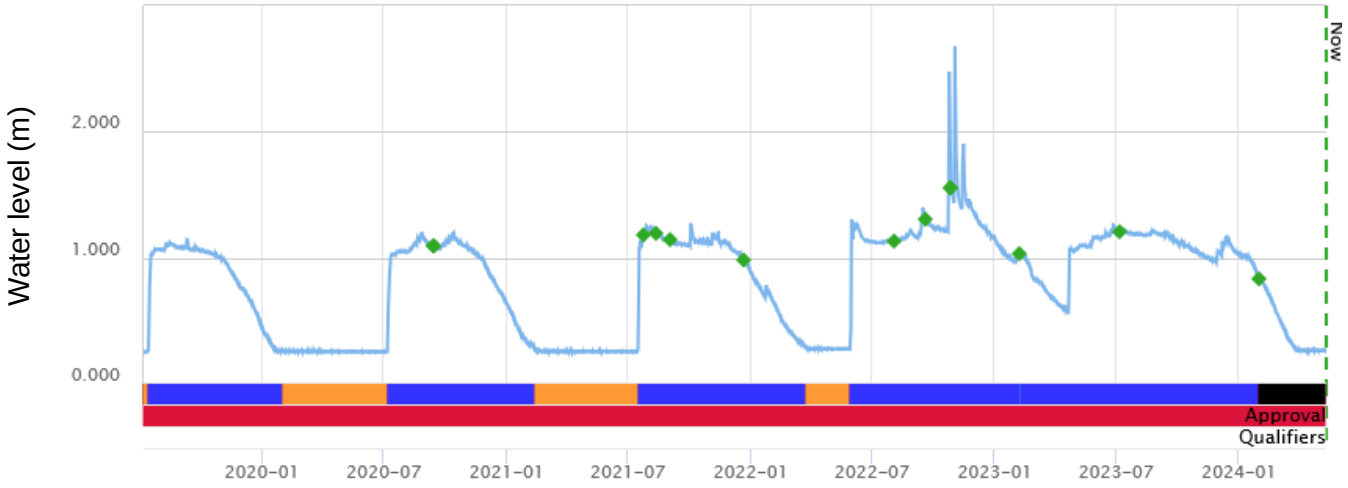

Figure 25. "Light River downstream Hamley Bridge" (LR2) station hydrograph. Minimum recordable value: 0.265 m. The green rhombuses represent the water level observed during field visits.

The orange sections of the hydrographs, where the lines are flat, are the entries where the water level was below the minimum recordable value. The hydrographs show stepwise seasonal fluctuations except for the "Wakefield River near Rhynie" station. This one shows a steadier water level. Given that the model is steady state, an effort was made to simulate the perennial transects of the rivers as a boundary condition. To achieve this, the missing water level records had to be filled to have continuous data to calculate the long-term average water level of each station. The methodology to do this was to approximate the hydrographs recession curve with a linear function for each period with a gap. Figure 26 shows an example of how the first gap was filled of the "Wakefield River upstream the Rocks" station. Although a linear function might not be the best to approximate the shape of the recession curve of the hydrographs, it was used because of its simplicity and its capacity to reach a value of 0 to represent a dry stream, something a plain exponential function can't do.

Once all the data gaps were filled, the average daily water level of each station was calculated. In ModelMuse, the bottom of the river was set to be the minimum topographic value read from the DEM

for each grid cell. With respect to the river stage, for the cells that only had a station downstream from them (and none upstream), it was set to be the river bottom plus the average water level calculated of the downstream station. For the cells that were between two stations (one upstream and one downstream), the stage was set to be the river bottom plus the average of the average water levels of both stations. Lastly, for the cells that only had a station upstream from them, the stage was set decrease gradually from the cell with the station to the last cell of the perennial transect. The initial riverbed conductance was set to be equal the K_V of the top layer (Hindmarsh Clay, a value of 3.1×10^{-4}). For the riverbed thickness, the default value of 1 m was used, and the river width was estimated with satellite imagery, the typical value was 10 m. The extent of the perennial river transects are shown in Figure 27.

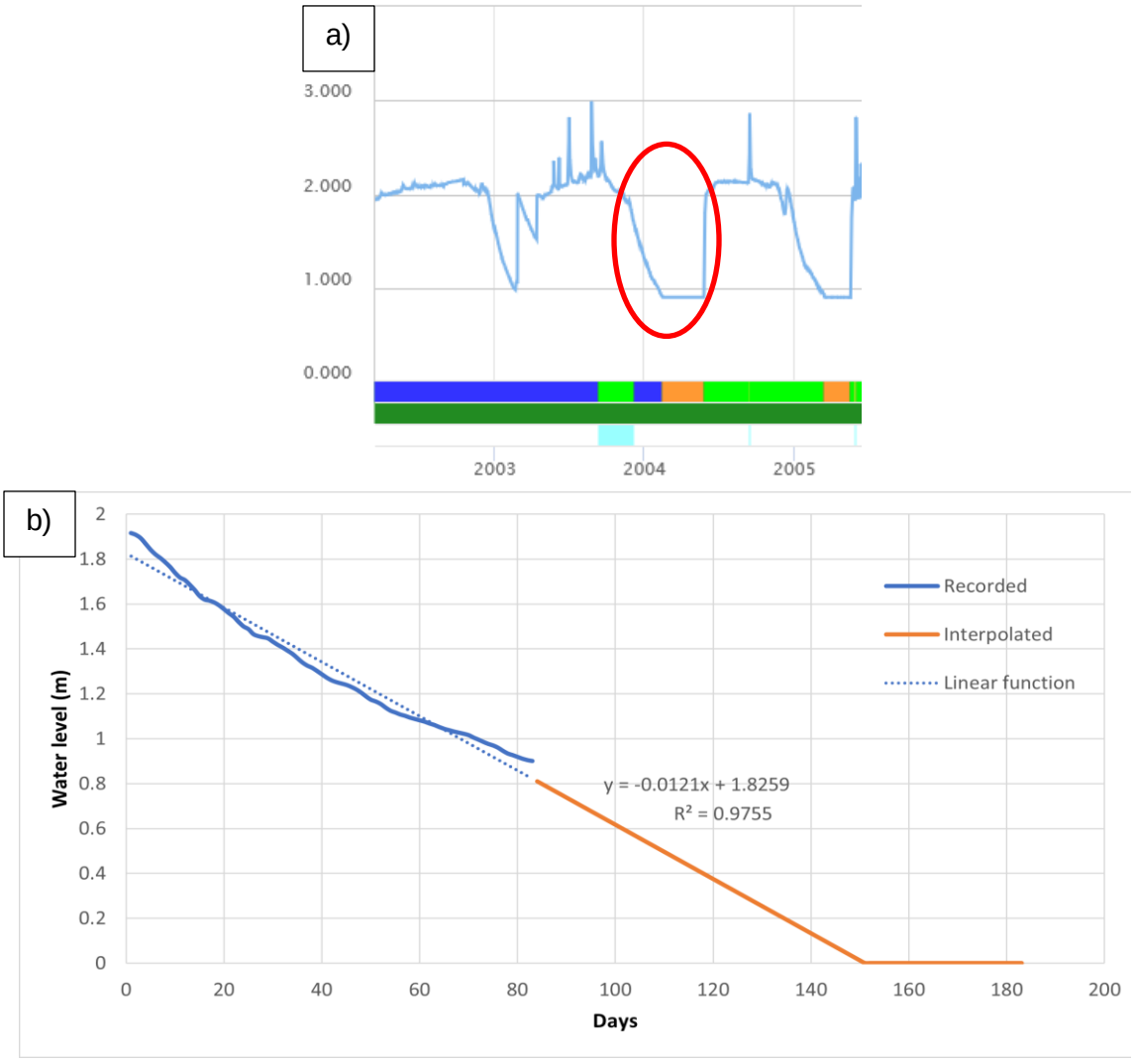

Figure 26: a) The data gap; b) Linear function used to approximate the recession curve.

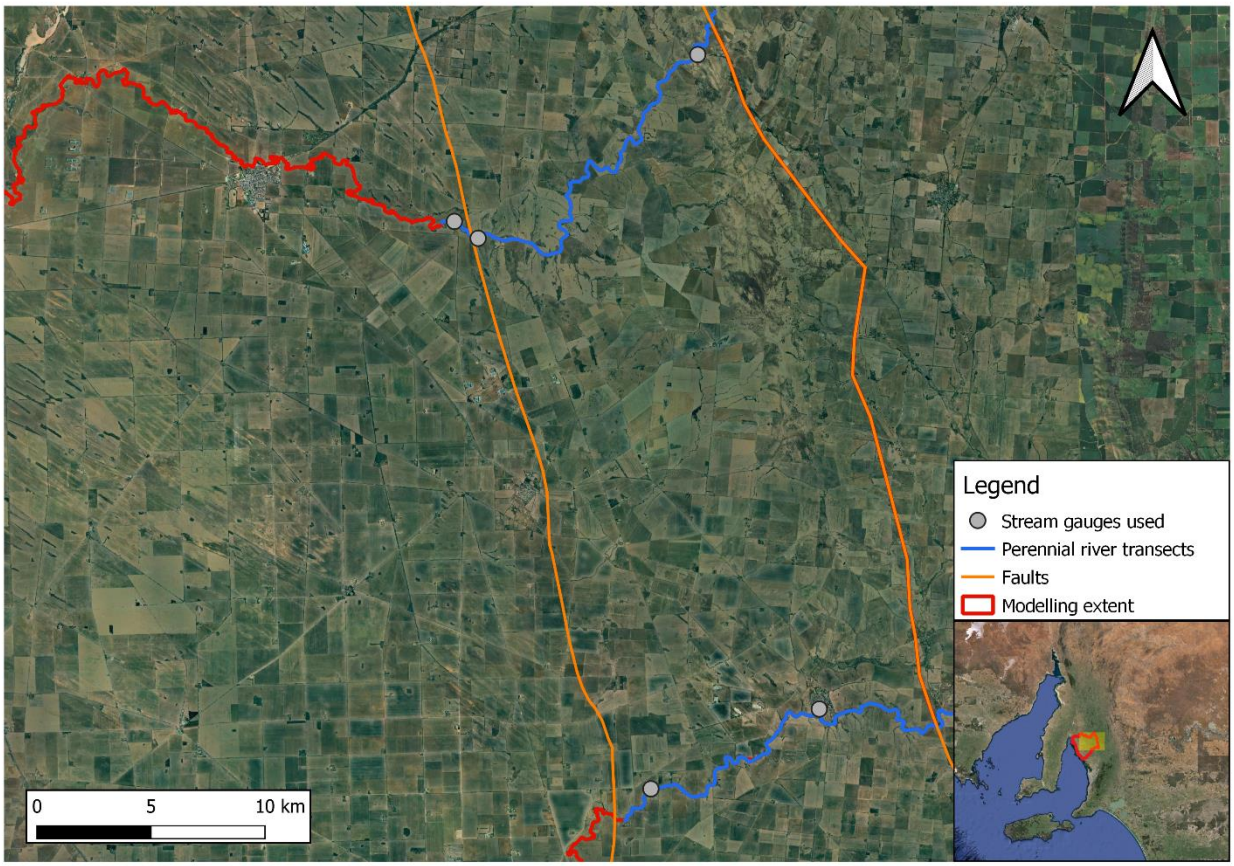

Figure 27. Perennial river transects simulated and stream gauges used.

2.3.3 Recharge

Net recharge was calculated using rainfall and actual evapotranspiration (ET) datasets from SILO (gridded data) and CMRSET 2.0 algorithm (Guerschman *et al*, 2022), respectively. Both datasets are the average annual values between 2000 and 2023.

The net recharge raster obtained by subtracting ET to the rainfall contained positive and negative values, meaning that some areas of the model domain gain water (water infiltrates into the subsurface), while some will lose (water leaves the subsurface via ET). However, some negative values were high, especially by the ocean boundary where the marshes and some tidal water bodies are located, and net recharge was up to -0.003 m/day (i.e., -7.5 m^3/day). Since the model doesn't account for the tidal fluctuation because it's a transient feature, the net recharge raster was further refined by removing those areas with high negative values. Figure 28 shows the final net recharge raster.

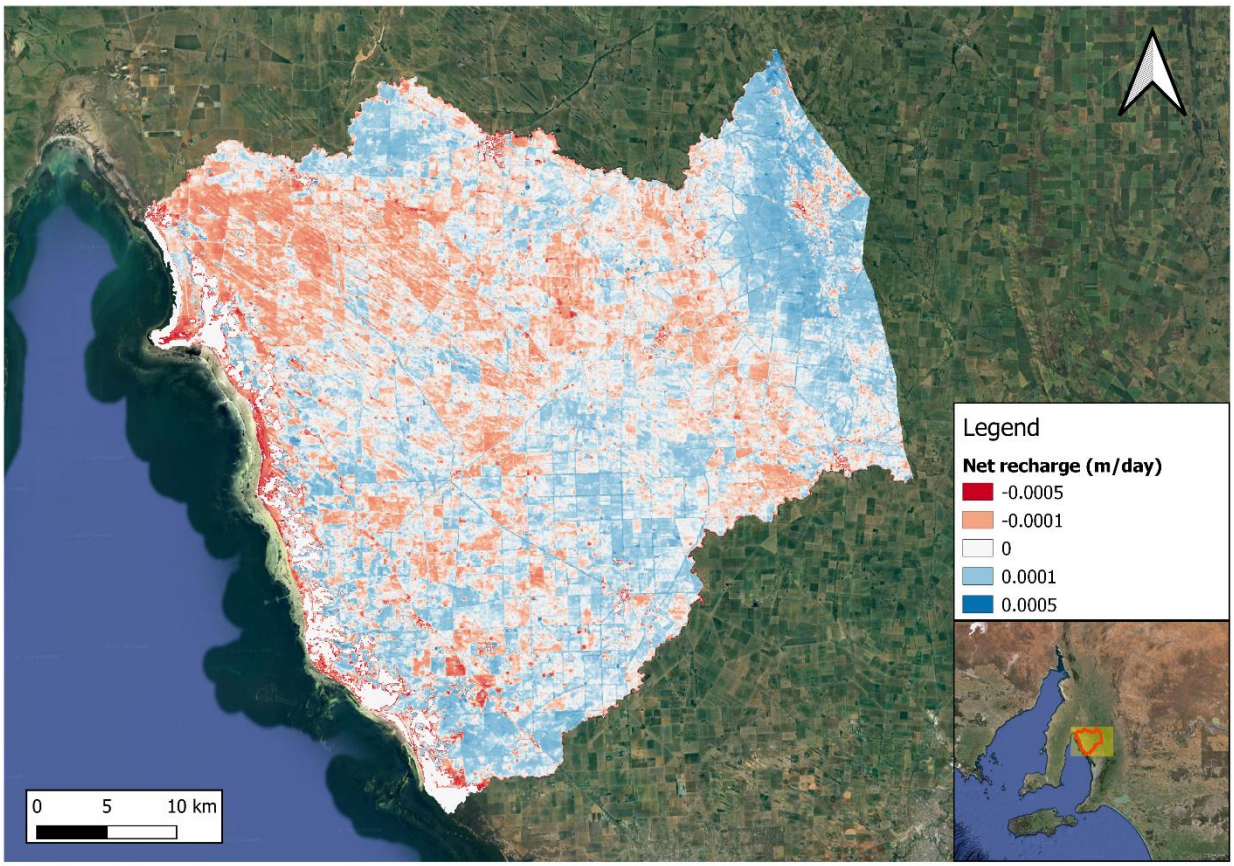

Figure 28. Net recharge (rainfall minus actual evapotranspiration) in the study area.

The net recharge raster was separated in two datasets: one with all the negative values to be simulated with the evapotranspiration package (EVT), and the other with all the positive values to be simulated with the recharge package (RCH). The EVT package requires an evapotranspiration extinction depth (ED) to indicate the distance from the model top at which the ET will be zero. This was obtained based on the reported values by Shah *et al* (2007) for different soil textures and land covers. The land cover of the study area is already explained in Section 1.5. The surface soil texture was obtained from a vector dataset published by the Department for Environment and Water (DEW) and is available at https://data.sa.gov.au/data/dataset/surface-texture.

The soil textures were matched to evapotranspiration extinction depths for grass landcover (shallow-rooted vegetation) because this is the closest to the dominant land use in the NAC, and the weighted average was calculated depending on their areal coverage. Table 6 shows the relevant data for the calculation of the extinction depth. The average ED assigned to the top layer of the model was 3.6 m.

Table 6. Determination of the extinction depth.

Dataset soil class	Coverage of the study area (%)	Extinction depth (m)*	Contribution of ED
D (loam)	39.77	3.7	1.472
F (clay loam)	21.77	5.05	1.100
C (sandy loam)	20.31	2.3	0.467
AF (sandy loam)	9.27	2.3	0.213
A (sand)	1.48	1.45	0.021
G (clay)	1.57	7.15	0.112
FF (clay)	0.79	7.15	0.056
EC (sandy clay loam)	1.02	3	0.030
E (sandy clay loam)	1.89	3	0.057
CF (loam)	0.07	3.7	0.002
BF (loam)	1.90	3.7	0.070
B (loamy sand)	0.16	1.7	0.003
Sum	**100**	**-**	**3.603**

*from Shah *et al* (2007)

2.4 Hydraulic head observations

In the study area there's only one active groundwater monitoring network, which is located around the Balaklava township. This network has 17 observations wells with water level data from as early as 1980 to April 2024, but only 11 of the wells are within the study area. The measurements are taken twice a year, approximately every 6 months. Unfortunately, these 11 observation wells don't provide a good spatial coverage of the study area because, like it was mentioned before, they're concentrated around Balaklava. Due to the poor spatial coverage of water level data, six new water level measurements were taken during fieldwork activities between November 2023 and March 2024 from other suitable groundwater wells that were identified in an attempt to improve the spatial coverage across the study area. These wells were selected because they hadn't been pumped for several years (minimum three years). Figure 29 shows the spatial distribution of the hydraulic head observations incorporated to the model, noting that there are still large areas without groundwater monitoring infrastructure.

Table 7 summarizes the relevant information about the water level observations that were used in the model. For the wells that are part of the observation network the average water level from 2000 to 2023 was used. With the respect to the vertical distribution, there are observations for the Hindmarsh Clay, Rogue and Clinton Formations, but not for the Carisbrooke Sand or the Port Willunga Formation.

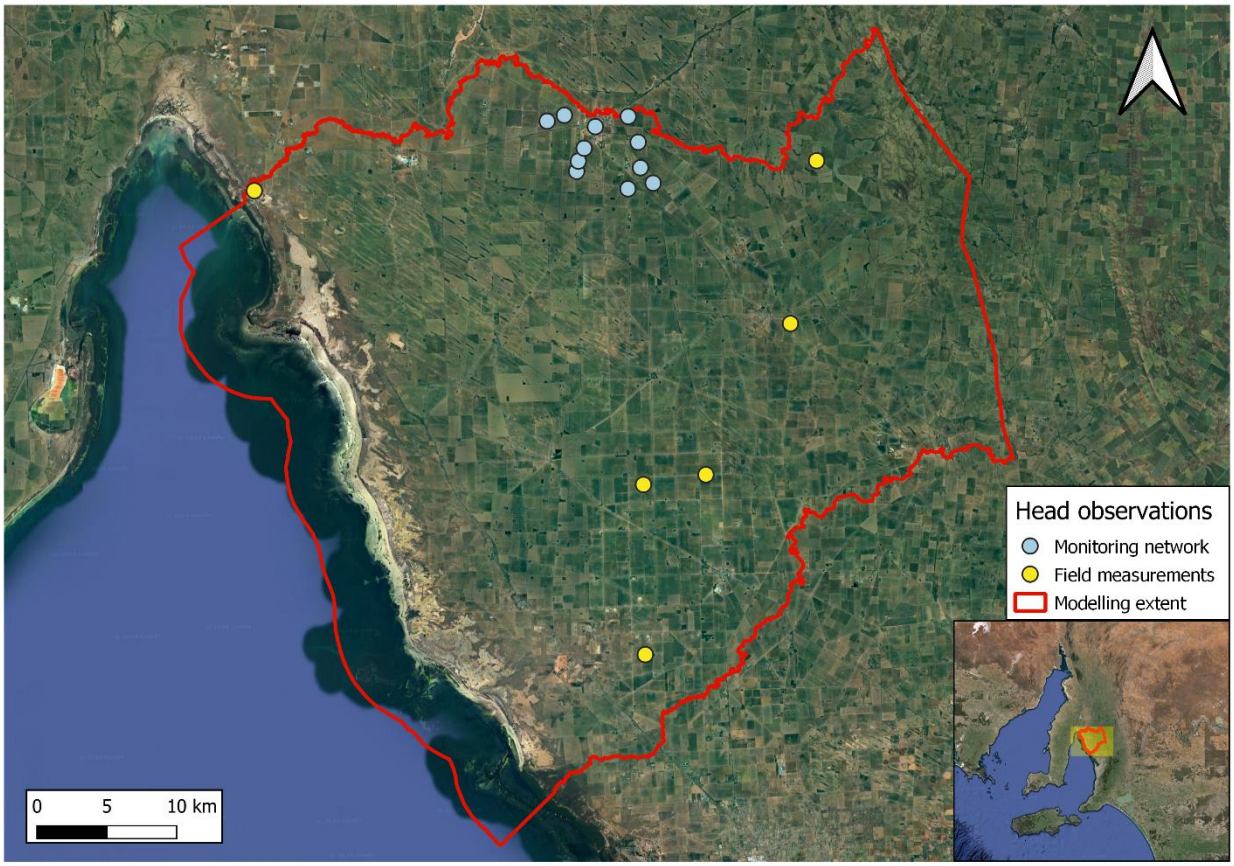

Figure 29. Spatial distribution of the groundwater hydraulic head observations in the study area.

Table 7. Details of the hydraulic head observations.

Observation well	Interval of years with data	Observed head (m AHD)	Aquifer	Model layer	Source
6529-492	1992 – 2023	62.01	Hindmarsh Clay and Rogue Formation (open hole)	1-3	Monitoring network
6529-127	1980 – 2023	54.67	Hindmarsh Clay and Rogue Formation (open hole)		
6529-540	1985 – 2023	49.87	Hindmarsh Clay, Rogue and Clinton Formations (open hole)	1-5	
6529-887	1993 – 2023	46.70	Clinton Formation	5	
6529-897		44.94			
6529-124	1980 – 2023	55.72	Hindmarsh Clay and Rogue Formation (open hole)	1-3	
6529-206	1985 – 2023	54.19	Hindmarsh Clay	2	
6529-466	1980 – 2023	55.18			
6529-543	1985 – 2023	55.79			
6529-172	1980 – 2023	46.67		1	
6529-219	1985 – 2023	51.04			
6529-23	30/11/2023	25.50	Clinton Formation	5	

6529-1147	28/11/2023	2.04	Hindmarsh Clay	1	Field measurements
6529-1185	27/11/2023	19.91	Rogue Formation	4	
6529-1066	18/3/2024	14.64	Hindmarsh Clay	1	
6629-2285	27/11/2023	91.00	Basement	4	
6629-2374	25/3/2024	142.86		3	

2.5 Model calibration

The automatic parameter estimation software PEST was employed for the model calibration. PEST implements an iterative gradient-search algorithm to minimize an objective function comprised of the sum of squared weighted residuals (i.e., the difference between model outputs and corresponding observations weighted by the degree of confidence associated to these observations) (Bresciani *et al*, 2015a). PEST was used in regularisation mode with singular value decomposition and Tikhonov regularisation as a measure to achieve uniqueness (Doherty and Hunt, 2010).

13 parameters were created and assigned to the hydraulic conductivities to calibrate them. Because of the lack of site-specific data and their natural ample ranges, hydraulic conductivities were allowed to vary three orders of magnitude below and above their initial values. The parameters used for calibration and their ranges are shown in Table 8.

Table 8. Parameters used for calibration.

Parameter name	Type	Layer or boundary condition affected	Lower bound (m/day)	Upper bound (m/day)
K	K_H	3 (Port Willunga Formation)	$6.3x10^{-4}$	630
Kv	K_V		$6.3x10^{-5}$	63
K1	K_H	1 and 2 (Hindmarsh Clay)	$3.1x10^{-6}$	3.1
Kv1	K_V		$3.1x10^{-7}$	0.31
K3	K_H	2 (Carisbrooke Sand)	$5x10^{-3}$	5,000
Kv3	K_V		$5x10^{-4}$	500
K4	K_H	3 and 4 (Rogue Formation)	$5x10^{-5}$	50
Kv4	K_V		$5x10^{-6}$	5
K5	K_H	5 (Clinton Formation)	$5x10^{-4}$	500
Kv5	K_V		$5x10^{-5}$	50
K6	K_H	3, 4 and 5 (Basement)	$1x10^{-6}$	1
Kv6	K_V		$1x10^{-7}$	0.1
Riverbed	Riverbed conductance (vertical)	Rivers	$3.1x10^{-7}$	0.31

2.6 Summary of the model setup

Table 9 summarises the relevant information of the MODFLOW model setup. The initial head across the entire model domain was set to be at the bottom of the first layer (around 20 m below the surface).

Table 9. Summary of the model setup.

Feature	Model layer	Initial K_H (m/day)	Initial K_V (m/day)	Time interval of the data used	To modify for calibration
Hindmarsh Clay	1 and 2	$3.1x10^{-3}$	$3.1x10^{-4}$		Yes
Carisbrooke Sand (Q4)	2	5	0.5		
Port Willunga Formation (T1)	3	0.63	0.063		
Rogue Formation (Teor)	3 and 4	0.05	0.005		
Clinton Formation (Teoc)	5	0.5	0.05		
Basement	3, 4 and 5	0.001	$1x10^{-4}$		
Constant head (equivalent freshwater head of the sea)	1 to 5				
Rivers	1		$3.1x10^{-4}$	All available data between 2000 – 2023	Yes
Recharge	Top of active layer			2000 – 2023	No
Evapotranspiration	Top layer (1) with an extinction depth of 3.6 m			2000 – 2023	No
Hydraulic head observations (17)	1 to 5			2000 – 2023 for 11 observations. One single measurement for the other 6	No

3. RESULTS

3.1 First simulation

The simulation prior calibration was unsurprisingly poor. The solver convergence criteria was not met and the root mean squared residual (RMSR) with respect to the head observations was very high for the 17 wells. The details of the first simulation are shown in Table 10. As it can be

appreciated, the modelled heads were significantly overestimated everywhere (high negative residuals).

Table 10. Result of the first simulation.

Head observation	Observed head (m AHD)	Simulated head (m AHD)	Residual	Solver convergence criteria	Water balance percent discrepancy	RMSR (m)
6529-492	62.01	72.59	-10.58	Not met	-0.02	1479.83
6529-127	54.67	91.63	-36.96			
6529-540	49.87	68.40	-18.53			
6529-887	46.70	58.39	-11.69			
6529-897	44.94	60.20	-15.26			
6629-2285	91.00	1,372.55	-1,281.55			
6629-2374	142.86	6,104.53	-5,961.67			
6529-124	55.72	81.46	-25.74			
6529-1066	14.64	114.60	-99.96			
6529-1147	2.04	3.06	-1.02			
6529-1185	19.91	131.65	-111.75			
6529-23	25.50	156.78	-131.28			
6529-206	54.19	57.85	-3.66			
6529-466	55.18	78.80	-23.62			
6529-543	55.79	64.30	-8.51			
6529-172	46.67	75.71	-29.04			
6529-219	51.04	58.18	-7.14			

3.2 Calibrated simulations

It was necessary to try several different calibration settings because the first calibration attempts were unsuccessful either because of numerical instability errors or unrealistic water table elevations in some areas of the model domain (artesian conditions for example). Moreover, it was noted that MODFLOW struggled to meet the solver converge criteria with the provided ET dataset. Many different solver settings were tested in an attempt to fix the problem, but the calibration results were still unsatisfactory. Because the model did not converge, a different approach was used – instead of feeding the model the positive and negative values of the net recharge dataset simultaneously, the areal average net recharge (positive values minus the negative values of the raster described in Section 2.3.3) would be used as the input. This approach resulted in a net recharge of 2.38×10^{-6} m/day across the entire model domain, and is equal to 0.22% of the rainfall. With this modification, the simulations were able to meet the solver convergence criteria and better calibrations were achieved.

It was also noted that the model performed better when the K_V values were not independently calibrated and just set to be 1/10 of the K_H. Therefore, for comparison purposes, the best model calibrations for four different model settings are presented in this section (see Table 11).

Table 11. Summary of the best model calibrations for different model settings.

Model setting	Solver convergence criteria	Water balance percent discrepancy	RMSR (m)	Number of iterations performed by PEST	Water table issues
ET included, K_V calibrated independently (ET-Kv)	Met	0.00	4.98	18	Skewed towards underestimation west of the Redbanks Fault (16/17 positive residuals), but artesian conditions east from it and squiggly contours for layers 1-3. High head differences between adjacent cells (up to 300 m)
ET included, K_V **not** calibrated independently (ETm)	Not met	-0.28	4.71	12	Squiggly contours and artesian conditions scattered in the southwest part of the region
Net recharge only, K_V calibrated independently (NR-Kv)	Met	0.00	4.69	14	Rivers are losing streams instead of gaining, and a small artesian area near the shore in the northwest
Net recharge only, K_V **not** calibrated independently (NR)	Met	0.00	2.52	15	Squiggly contours near the Redbanks Fault for layers 1-3. A small artesian area near the shore in the northwest

The goodness of fit of each calibrated model setting with respect to the individual values of the head observations are shown in Figure 30. Note how most of the simulated heads of ET-Kv (blue rhombuses) are below the 1:1 line (perfect match) meaning that the water table is underestimated with respect to the observations. There's not much difference between the other three model settings except for a couple of points, still, the "best" calibration was achieved with NR not only because of the lowest RMSR, but also because the water table was the most realistic one without contradicting the input data (unlike how NR-Kv made the rivers losing streams instead of gaining).

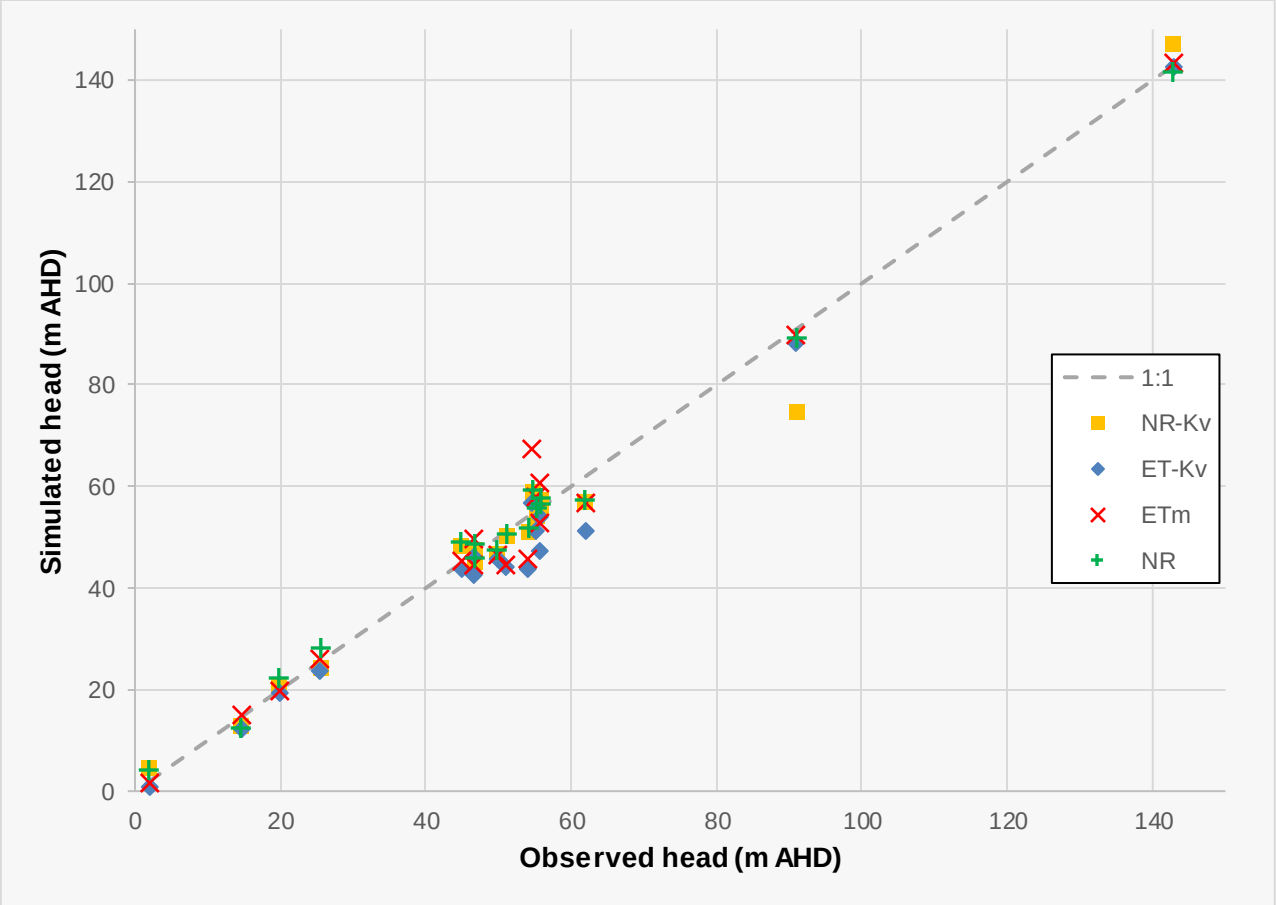

Figure 30. Simulated vs observed heads for the different calibrated model setting.

3.2.1 Calibrated parameters

The calibrated hydraulic conductivity values of the NR model are shown in Table 12. Four parameters decreased and three increased with respect to their initial values, but none of them reached either the upper or lower limit. The parameter with the biggest increase was the Hindmarsh Clay K_H (154.5 times) while the largest decrease occurred for the Rogue Formation K_H (2.62×10^{-3}). The units order, from highest to lowest K_H, is as follows: T1, Q4, Hindmarsh Clay, Teoc, basement and Teor.

Table 12. Calibrated values of the NR model and their change factor with respect to their initial values.

Hydrostratigraphic unit	K_H (m/day)	Change factor	K_V (m/day)
Hindmarsh Clay	0.479	x154.5	4.79×10^{-2}
Carisbrooke Sand (Q4)	0.67	x0.134	6.7×10^{-2}
Port Willunga Formation (T1)	2.139	x3.395	0.214
Rogue Formation (Teor)	1.31×10^{-4}	x0.00262	1.31×10^{-5}

Clinton Formation (Teoc)	0.133	x0.265	$1.33x10^{-2}$
Basement	$2.826x10^{-2}$	x28.26	$2.826x10^{-3}$
Riverbed conductivity		x0.0133	$4.123x10^{-6}$

3.2.2 Parameter sensitivity

PEST calculates the composite sensitivity of the parameters during every iteration based on the observation and prior (initial) information. The composite parameter sensitivities of the best iteration of the NR model were normalized and are shown in Figure 31. The most sensitive parameter resulted to be the basement hydraulic conductivity (k6), followed by the Hindmarsh Clay conductivity (k1), and later by the Clinton Formation conductivity (k5). On the other hand, the parameters that had the smallest impact on the model are the riverbed conductance, the Rogue Formation and the Carisbrooke Sand conductivities (k4 and k3, respectively).

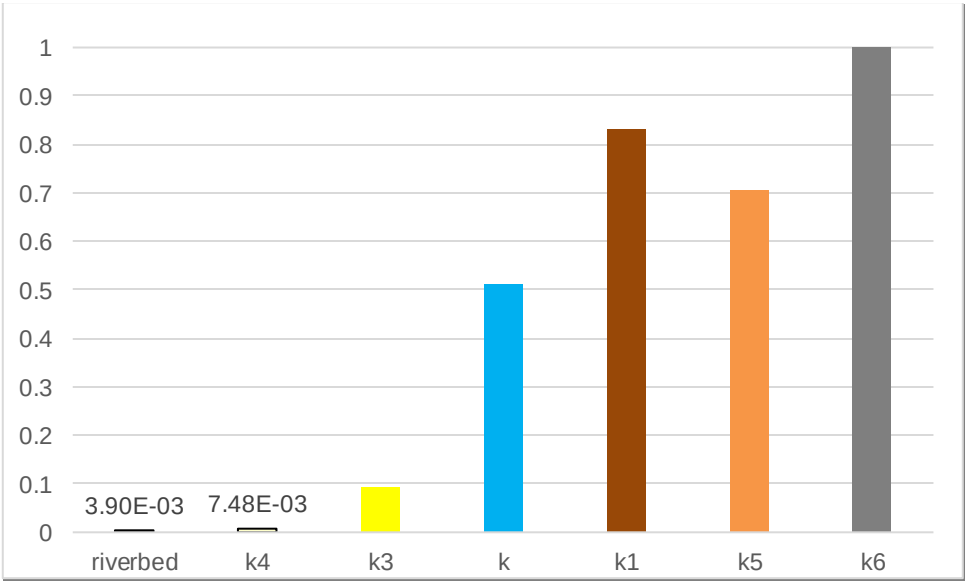

Figure 31. Normalized composite parameter sensitivities of the NR model.

The parameter k6 turned out to be the most sensitive probably because this is the hydraulic conductivity that controls the gradient, and therefore, the flow rate between the mountain block and the Tertiary units, significantly affecting the water balances of three hydrostratigraphic units – the basement, Rogue and Clinton Formations (see sections 3.2.3 and 3.2.4).

3.2.3 Hydraulic head distribution

The water contours of each layer of the NR model are shown in Figure 32. In this figure three main things can be appreciated:

1. The general flow direction obeys the topography: starts from the northeast section of the study area going southwest until it reaches the Redbanks Fault where it makes a slight change in direction more towards the west to finally discharge at the sea.

2. Overall, all contours present almost no variation between layers, meaning that they're in hydraulic connection and in equilibrium, as expected from a steady-state model.

3. The only portion with significant variation in the contours (squiggly lines) is in the transition from the basement to the Rogue Formation because of a drastic change in hydraulic conductivity of two orders of magnitude (see Section 3.2.1)

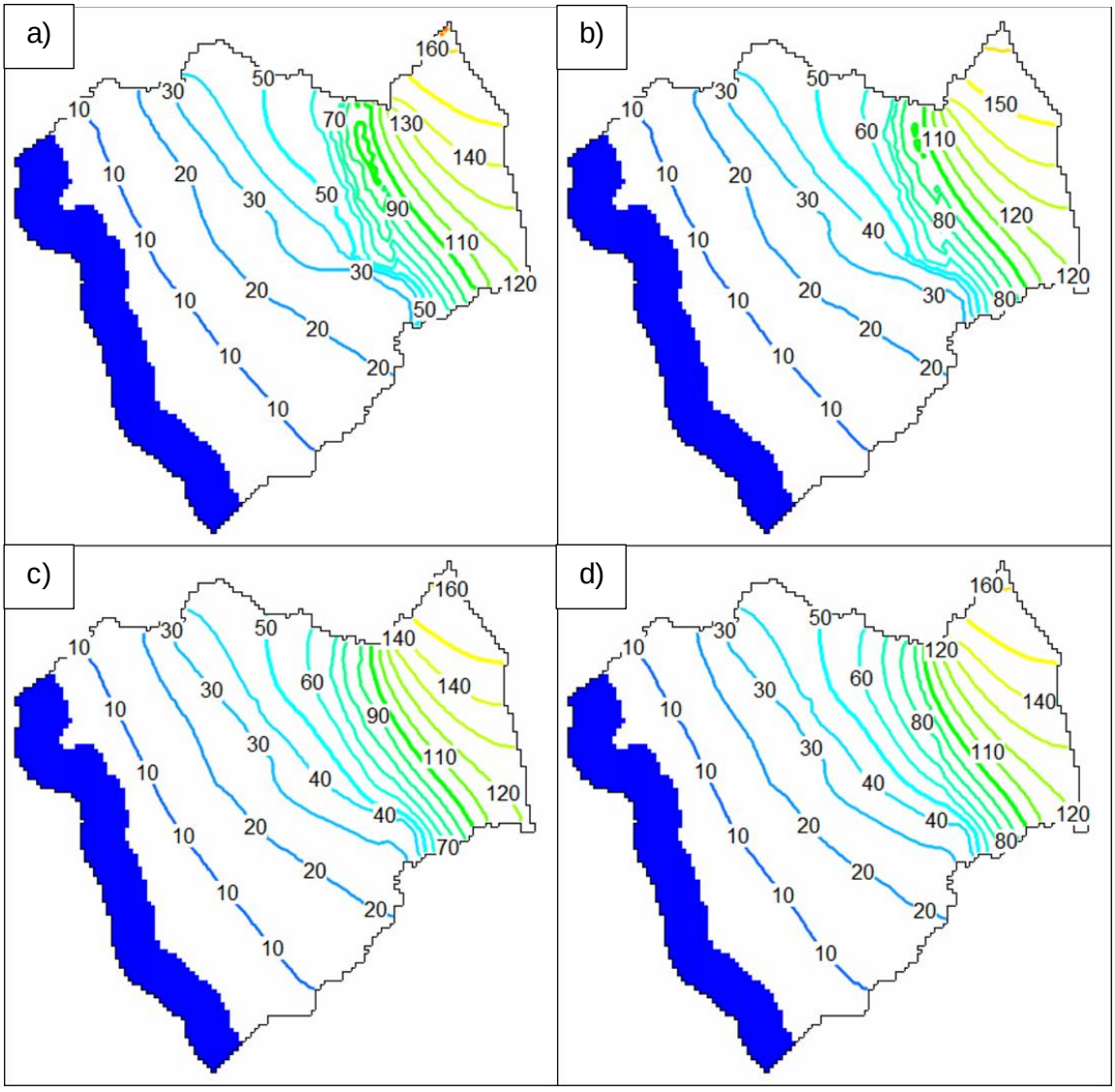

Figure 32. Water table contours (m AHD) of: a) the Quaternary unit (first two layers of the model); b) the third layer; c) the fourth layer; and d) the fifth layer. The blue polygon represents the sea.

Point number three above can be explained taking a closer look at the head distribution and layers hydraulic properties. Figure 33 shows a close-up view of this zone from three different perspectives. They water contours turned out to be like this because the transition from the basement to the Tertiary units. The contours are straight lines while they're still in the basement because K doesn't vary with depth, however, as soon the water table crosses the Redbanks Fault, the hydraulic properties do change with depth, causing the contours to deflect (see Figure 33b and 33c). The

water flowing through the Rogue Formation experiences a retardation because of its low K_H (1.31×10^{-4} m/day) compared to the rest of the layers. As a result, vertical water flow is promoted and directed downwards at the beginning because the underlaying unit, the Clinton Formation, is three orders of magnitude more conductive (K_H = 0.133 m/day), but later the cavity of the contours gets inverted as the Rogue Formation narrows, promoting the flow upwards. So, the Rogue Formation is an aquitard according to this model, water avoids circulating horizontally through this unit because of its low conductivity.

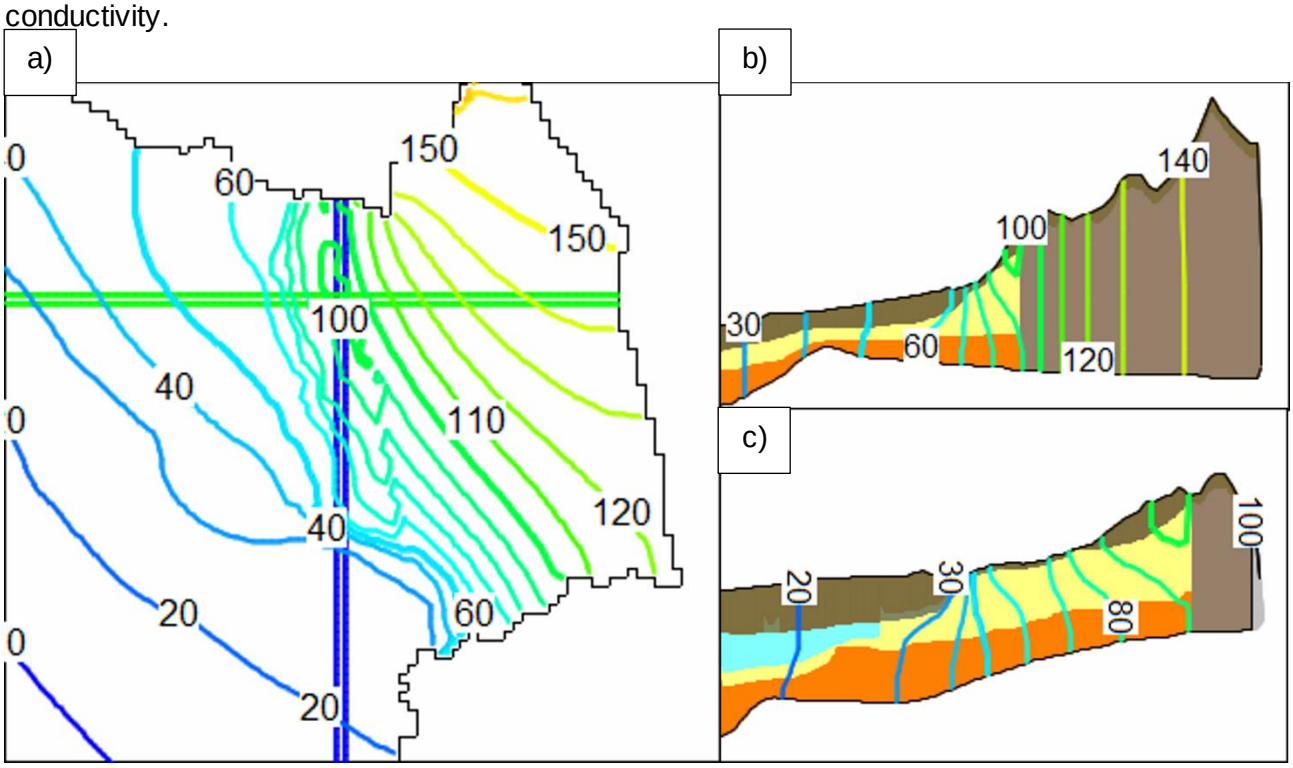

Figure 33. Close-up view of the squiggly contours: a) top view of the top layer; b) front view (green bar); and c) side view (blue bar). Note how the contours are not so deflected in the Port Willunga Formation (light blue polygon in the side view).

3.2.4 Water balance

The fluxes between hydrostratigraphic units and boundary conditions were determined using the ZONEBUDGET utility of MODFLOW. All the fluxes for every unit including the boundary conditions are shown in Table 13. In this matrix, the numbers mean a flow from the feature in the row to the feature in the column. For example, row HC (Hindmarsh Clay) and column Q4 (Carisbrooke Sand) reads 1,761 (m^3/day), which means that HC lost that volume of water and Q4 gained it each day. The blank cells mean that there's no water exchange between the features.

Table 13. Interaction matrix in m^3/day

Unit	HC	Q4	T1	Teor	Teoc	Basement	Rivers	Sea
HC		1,761	1,674	222		998	7	1,196
Q4	1,074		1,116	41		8		
T1	195	349		235				2,498
Teor	224	130	363		494	2		0.24

Teoc				714		2		462
Basement	204		123	1	682			
Recharge	4,157							
Rivers	4							
Sea	1							

The net fluxes matrix is shown in Table 14. Here, a negative number means that the attribute listed in the column lost water to the attribute listed in the row. Some of the cells were left out to avoid the duplication of values. According to this matrix, T1 receives a recharge of 2,497 m^3/day of which 90% comes from the Quaternary unit (59% from the HC and 31% from the Q4). Teor receives 220 m^3/day as recharge that come entirely from Teoc. Lastly, the latter receives a recharge of 680 m^3/day coming entirely from the basement. So, for the T1 the dominant recharge mechanism is mountain front, whereas for Teor and Teoc is mountain block, according to this model. Also, the negative numbers in the Teor and Teoc columns imply that the general flow is upwards from these Tertiary units to the overlaying layers.

Table 14. Net fluxes matrix m^3/day

Unit	HC	Q4	T1	Teor	Teoc	Basement	Recharge	Rivers	Sea
HC		687	1,479	-2		794	-4,157	4	1,195
Q4			767	-89		8			
T1				-128		-123			2,498
Teor					-220	0.34			0.24
Teoc						-680			462

3.2.5 Travel times

Travel times were estimated using MODPATH 6. Five groups (one per layer) of nine water particles each were deployed to calculate the time it would take them to reach the sea. To do this, the backward tracking option was selected, and the initial placement of the particles was on the left face of a cell just right to the sea boundary condition. Figures 34 to 38 show the pathlines of each group of particles and the calculated times. The pathlines are represented by the rainbow-coloured lines in the figures. All the groups of water particles end in the same row and column of the model as the one shown in Figure 34a and 34b, the only difference is the layer (or depth) at which they reach the sea.

In Figure 34 the travel times determined by the model may seem excessive because of the relative short length of the pathlines, however, it is worth noting that the distance that the particles travelled isn't that short. The pathlines span diagonally across little more than four cells and each one has a diagonal length of 707.1 m, so, they travelled roughly a distance of 2.83 km. And this is the 2D distance only, it's actually more than that because the particles move in all three dimensions. Nonetheless, the distance alone isn't enough to determine the travel time of the particles, the other

and very important component is the gradient. The head difference between the beginning of the pathline and its end is of 2.5 m, therefore, the gradient is around 2.5 m ÷ 2,830 m = 8.83×10^{-4}, which is indicative of a pretty flat water table.

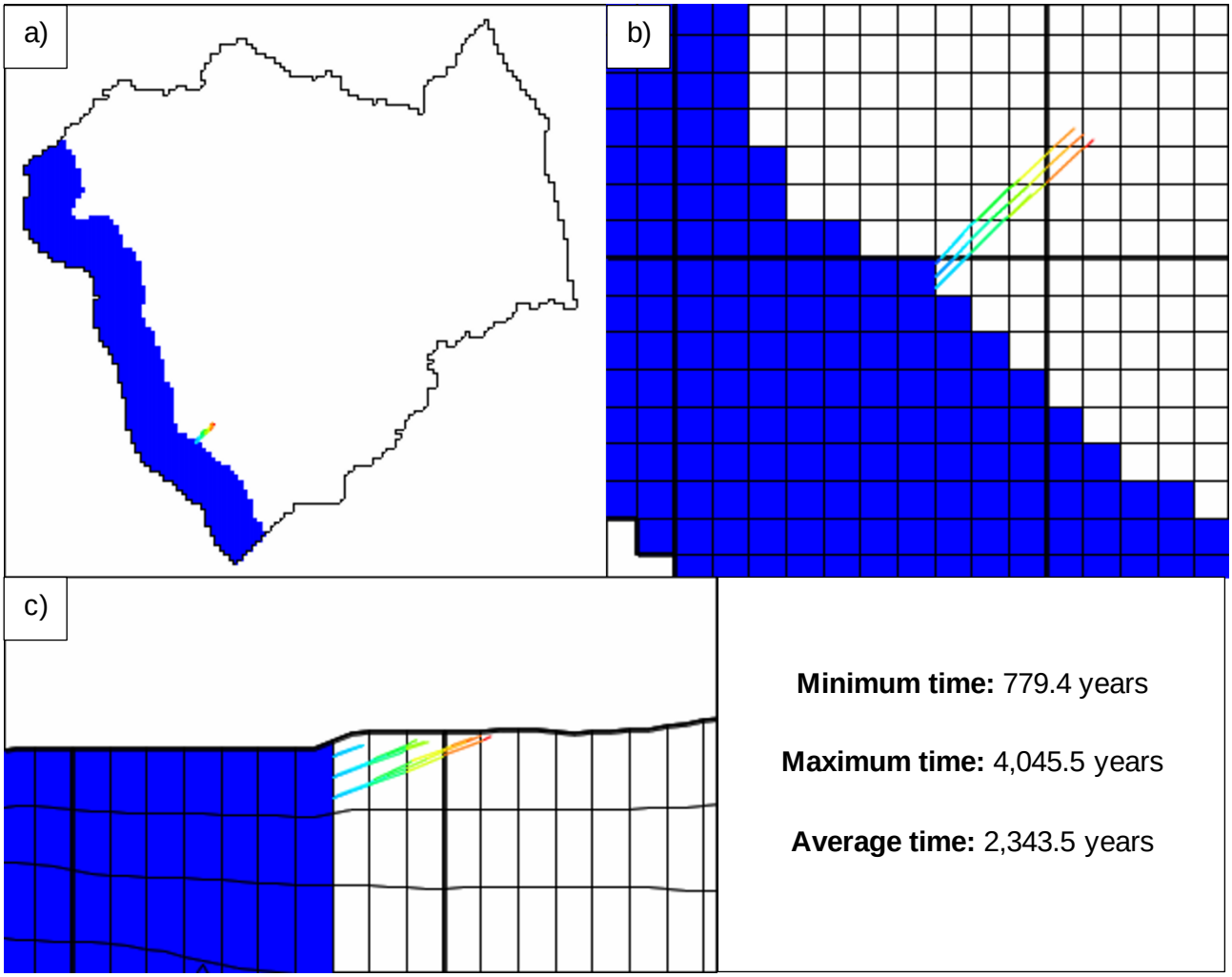

Figure 34. Pathlines for the group in the first layer: a) overview (top); b) close-up view (top); c) front view. The blue polygon represents the sea.

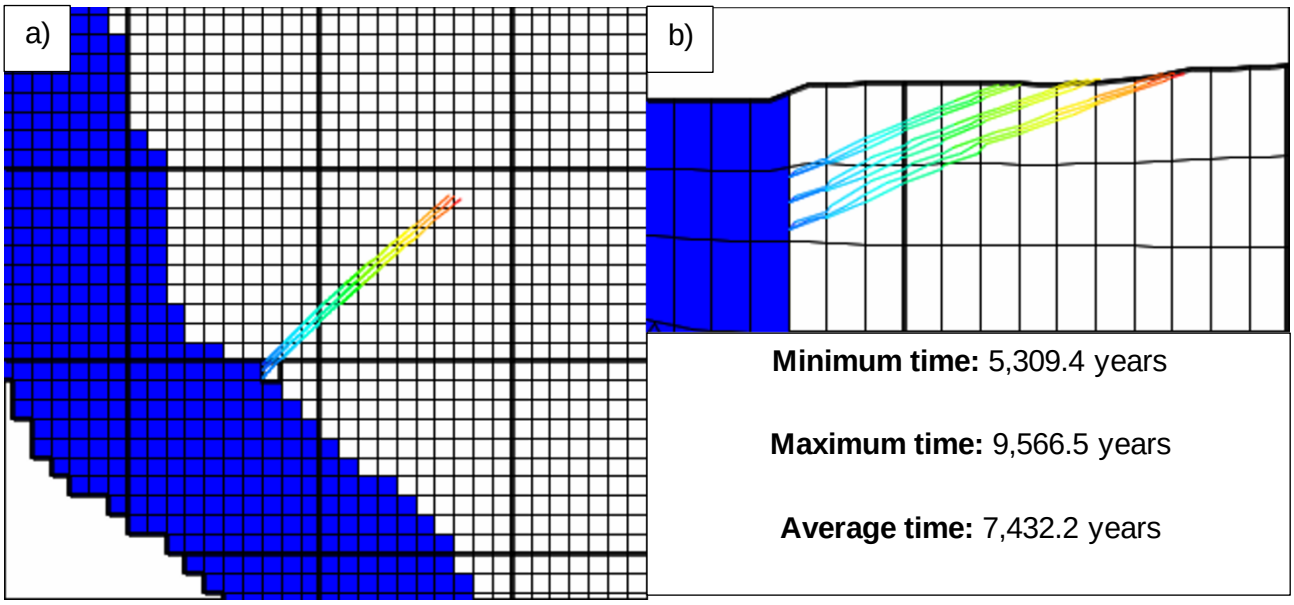

Figure 35. Pathlines for the group in the second layer: a) close-up view (top); b) front view.

There's a large increment in the length of the pathlines in layer 3 (Figure 36) compared to layer 2 (Figure 35). Figure 36b is the front view of the 3D view of ModelMuse because the length of the pathlines didn't allow to display them properly in the 2D view of model. The same happens for Figures 37 and 38.

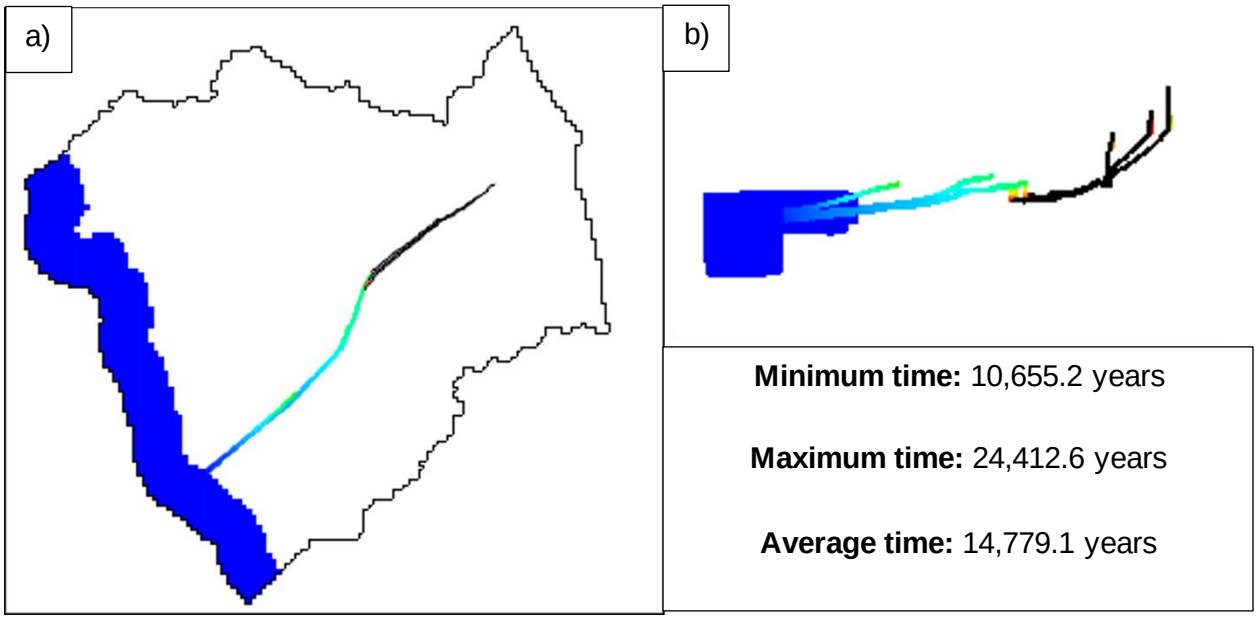

Figure 36. Pathlines for the group in the third layer: a) overview (top); b) front view. Note the big differences in particles pathways.

There's a considerable increase in the travel times of the group in layer 4 compared to the ones in layer 3: one order of magnitude bigger. This is because the very low K_H of the Rogue Formation (the fourth layer) of 1.31×10^{-4} m/day.

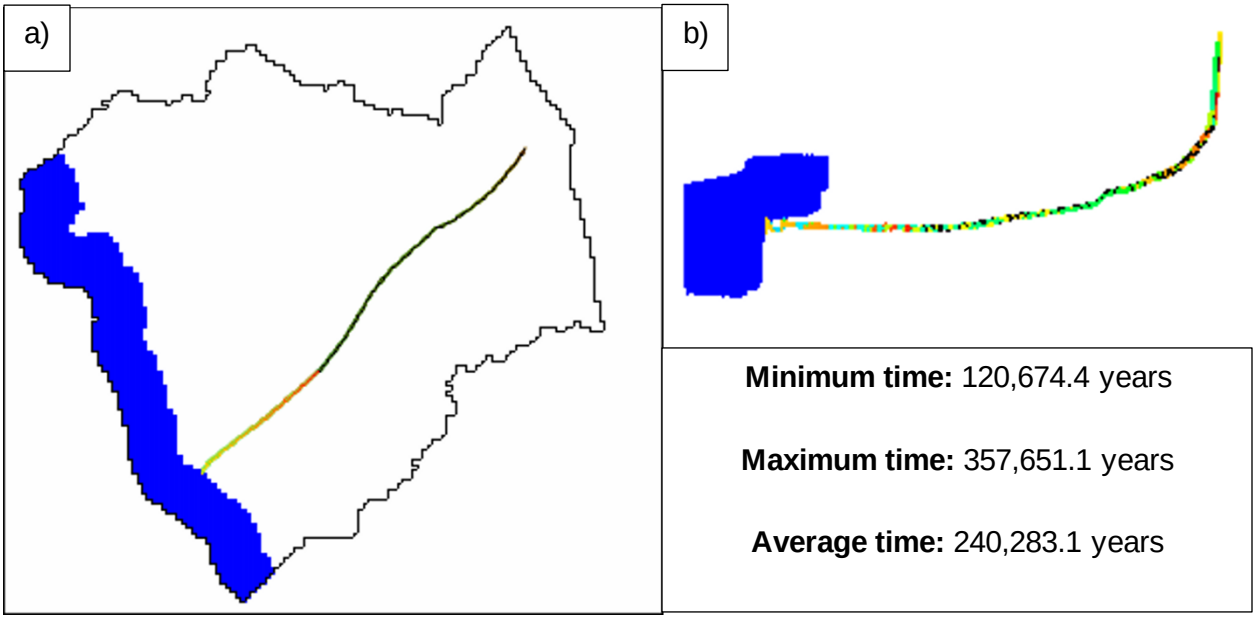

Figure 37. Pathlines for the group in the fourth layer: a) overview (top); b) front view.

Although, the pathlines of the group in layer 5 (Figure 38) seem about the same length as the ones in layer 4, the travel times are shorter because the Clinton Formation (layer 5) has a K_H (0.133 m/day) three orders of magnitude bigger than the Rogue Formation.

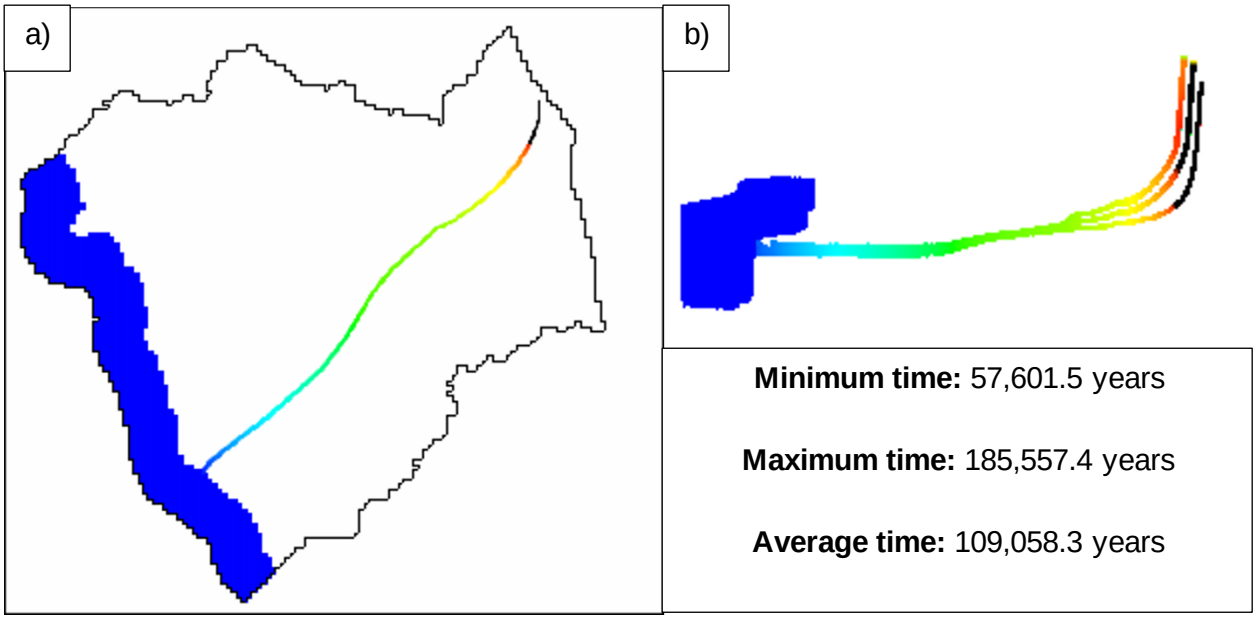

Figure 38. Pathlines for the group in the fifth layer: a) overview (top); b) front view.

4. DISCUSSION

Many challenges were encountered while developing this study, many of which became limitations and sources of uncertainty. The most relevant ones are described in this section.

4.1 Hydrostratigraphic information coverage

As presented in section 1.8, the hydrostratigraphic information used (which is a crucial component of the numerical model) is limited to point data, and in some parts of the study area, the density of records is low. Particularly, the southwest portion of the NAC has a very low density of bores with records for the Tertiary units.

In addition, the layering was simplified with the assumption that the Rogue Formation underlies the Quaternary unit and the Port Willunga Formation, and subsequently, the Clinton Formation underlies the Rogue Formation. In reality, the sequence of the layers is not homogeneous and the aforementioned assumption excludes direct contacts/interactions between layers like the Port Willunga and the Clinton Formations that could be important. More stratigraphic records along with areal stratigraphic information (such as the one obtained with many geophysical techniques) could considerably improve the accuracy of the model's layers.

4.2 Boundary conditions

4.2.1 River data

As mentioned in section 2.3.2, the river data presented a lot of gaps: mismatching records in time, records no longer than six years, unrecorded water levels, and unmeasured discharge. Adding the latter to the stream gauges operation could be very useful to determine losing or gaining transects by applying differential gauging, and it could also be used as another calibration dataset besides the hydraulic head observations, to contribute to the robustness of the model.

4.2.2 ET and recharge

The ET dataset used was particularly problematic because of the issues described in Section 3.2. A detailed examination of the CMRSET 2.0 algorithm might help to identify the source of the issues (if any). Alternatively, other methods that accommodate for the specific conditions of the NAC to estimate actual ET could be used, lysimeter for example.

The recharge dataset can also be improved using other methods to calculate it, for example chloride mass balance or the water table fluctuation method. Nonetheless, the value of recharge obtained was plausible, 0.22% of rainfall, and Bresciani *et al* (2015a) reported a calibrated value of recharge for the NAP of 0.08% of rainfall, but they discussed that that value is at the lower limit of the given calibration range.

4.2.3 Other boundary conditions

Lack of information such as groundwater extraction or artificial recharge, add to the uncertainty of the model. Although most of the agriculture in the NAC is seasonal, there's still groundwater irrigated agriculture, and groundwater extraction for domestic, stock and town supply. However, this information is not readily available.

4.3 Hydraulic head observations coverage

The limited hydraulic head observation coverage is one of the main concerns of the study. As commented in section 2.4, there enormous areas without a hydraulic head observation, and two hydrostratigraphic units (Port Willunga Formation and the Carisbrooke Sand) don't have a hydraulic head observation, causing bias. Moreover, six of the observations used as the calibration dataset are not long-term average like the other 11. A wider monitoring network that targets all the major units in a more equitable manner, can significantly enhance the accuracy and robustness of the model.

4.4 Calibrated parameters

The outcome of a PEST calibration strongly depends on the prior information of the parameters (initial values) and, ideally, the initial value of a parameter should be based on expert knowledge and/or field measurements. No site-specific data was used to assign the values of hydraulic conductivities of the units nor the riverbed conductance. At best, data from other studies nearby the NAC, such as Bresciani *et al* (2015a), was used for the initial values of the shared units like the Hindmarsh Clay and the T1 limestone (Port Willunga Formation). However, the Rogue and Clinton Formations are not present in that study, and no other sources of information were found with respect to their properties, making them more uncertain than the rest. Core samples and/or pumping tests performed in the NAC are required for a better-informed assignation of the initial values.

4.5 Hydraulic head distribution

The best model obtained (the NR model described in Section 3.2) presented small zones with artesian conditions. By comparing that area against satellite imagery it was found that most of the artesian cells are located on what seems to be dry water bodies (see Figure 39). Furthermore, the land use here corresponds to marshland/wetland (see Figure 5) and it's a local topographic depression bounded to the east and west as shown in Figure 39c. Therefore, it's likely that groundwater does discharge there (at least in most of the biggest polygon with artesian conditions), and that not all the artesian cells are a flaw of the modelled water table.

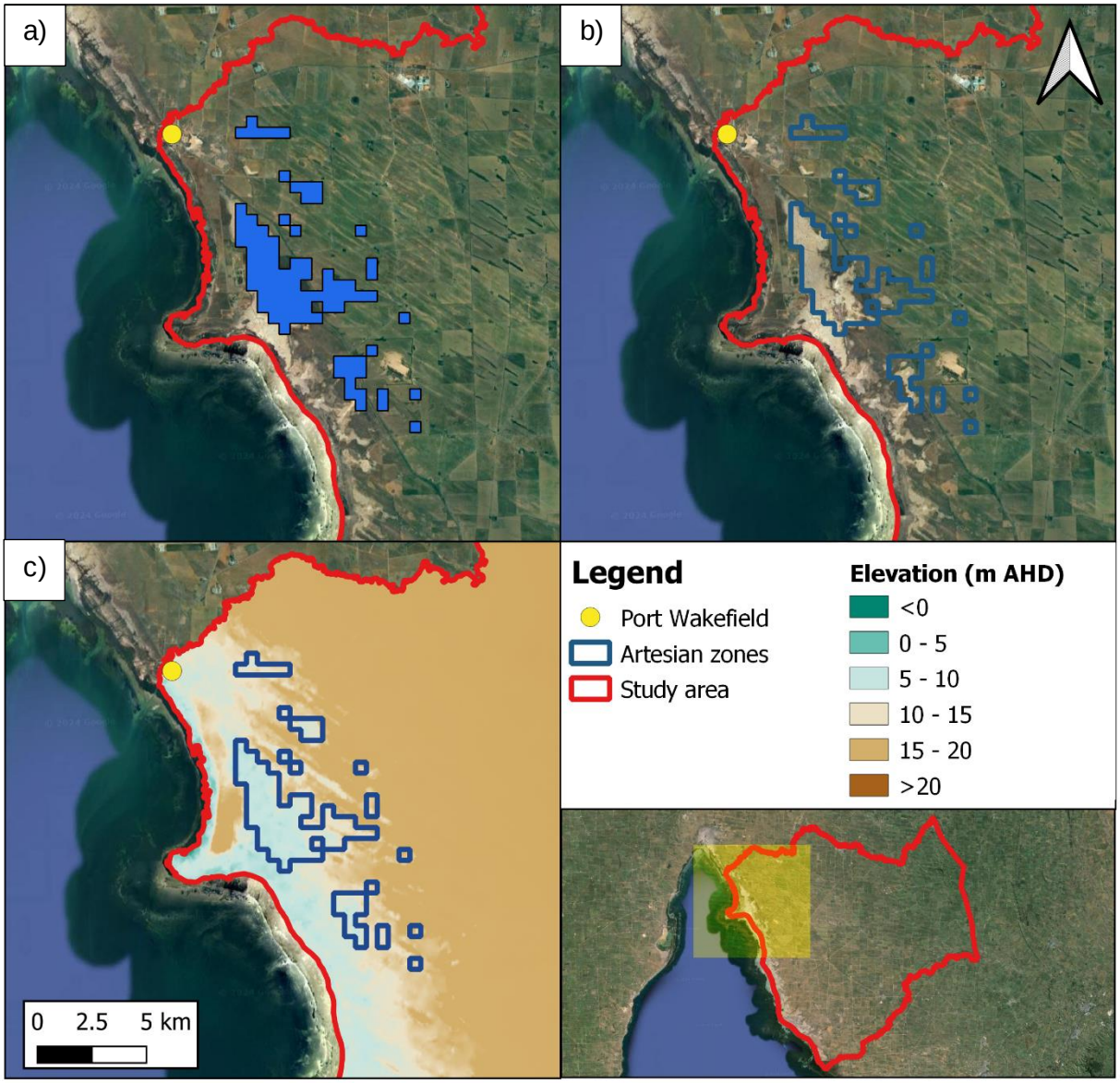

Figure 39. a) Location of the artesian cells of the numerical model; b) satellite imagery for the artesian cells; c) surface elevation.

Figure 40 shows two zoomed views of the biggest polygon to appreciate the drainage features present.

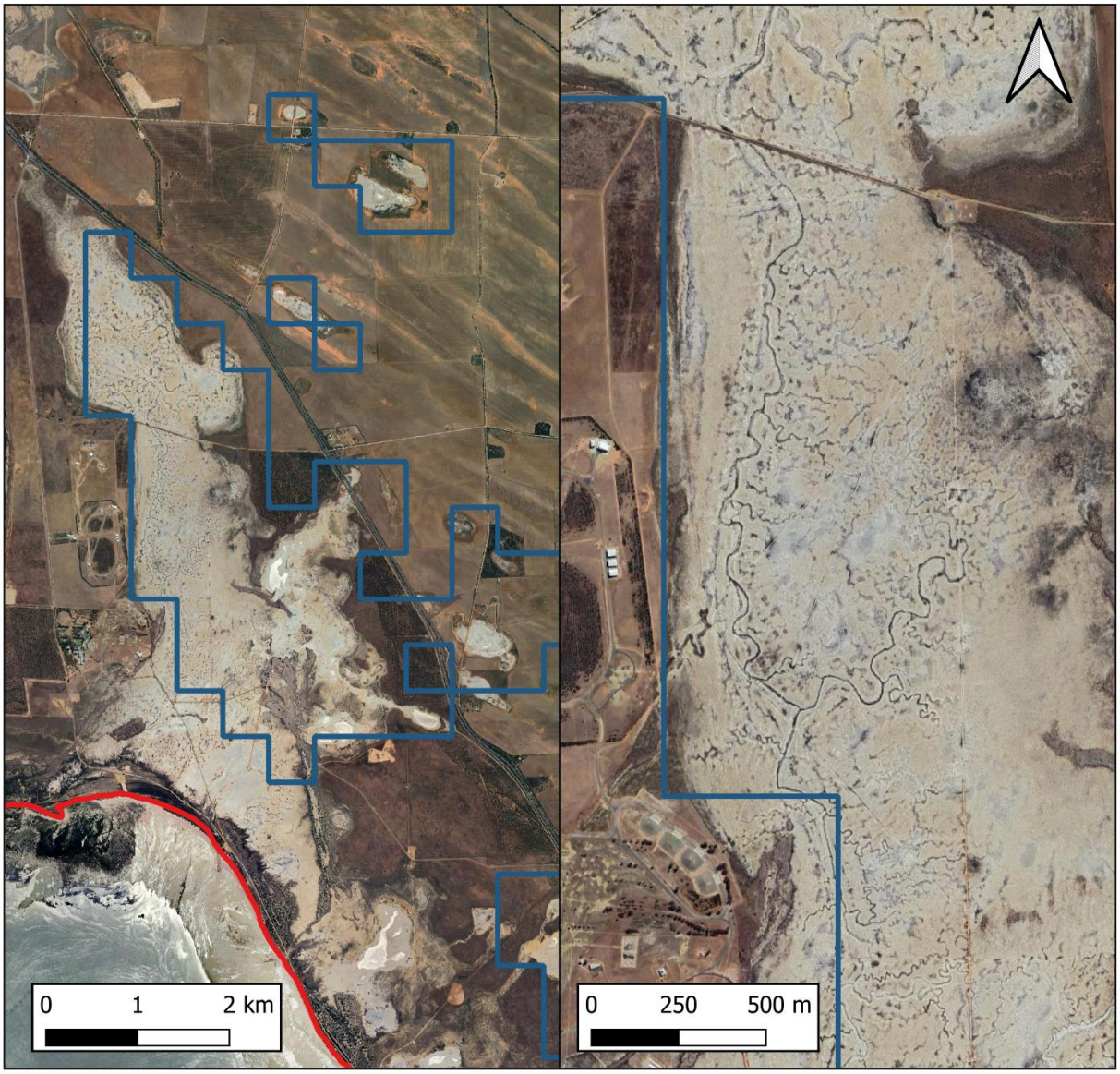

Figure 40. Zoomed views of the presumably groundwater discharge zone.

4.6 MODPATH travel times

The water travel times reported in Section 3.2.5, were calculated with MODPATH's default effective porosity (n_e) of 0.25 for all units given that no specific values of this property were available. Hence, those times are just an indicative of the possible ranges of the given pathlines that could be obtained under steady-state conditions. There's a lot of opportunity for improvement of this analysis, starting with specific values of n_e.

5. CONCLUSIONS

A conceptual model and a numerical groundwater model were developed for the Northern Adelaide Corridor. The stratigraphic information revealed that the confined Tertiary units (Port Willunga,

Rogue and Clinton Formations) do not extend past the Redbanks Fault. Moreover, the Port Willunga Formation does not extend completely across the NAC, it's restricted to the west and southwest of the study area. In the Mount Lofty Ranges, east of the Redbanks Fault, the basement takes over and goes near the surface. Here, the Quaternary presents a reduction in thickness reaching minimums of a few centimetres. The Wakefield and Light Rivers also presented significant differences across the NAC. East of the Redbanks Fault the rivers tend to be gaining streams, and the opposite is true when they are west from it.

The general groundwater flow direction, according to the computed hydraulic heads by the steady-state numerical model, is towards the southwest. The highest hydraulic heads are located in the northeast corner of the NAC, in the Mount Lofty Ranges, and the groundwater flows southwest until it reaches the Redbanks Fault, where it starts heading a little more towards the west to discharge at the sea. The hydraulic head distribution and water balances showed that the recharge for the Rogue and Clinton Formations is via lateral flow from the basement (Mountain Block Recharge), whereas for the Port Willunga Formation 90% comes from the Quaternary unit via downward flow (Mountain Front Recharge) and only 10% via lateral flow. The estimated recharge for the NAC equals 0.22% of rainfall.

According to the calibrated K_H values, the Port Willunga Formation is the most conductive unit (2.14 m/day) followed by the Carisbrooke Sand (0.67 m/day). On the other hand, the least conductive units are the Rogue Formation (1.31×10^{-4} m/day, which makes it function as an aquitard), the basement (2.83×10^{-2} m/day) and the Clinton Formation (0.13 m/day).

Despite the limited calibration dataset (11 long-term average hydraulic head observations and 6 single measurements), a relatively good calibration was achieved (RMSR = 2.52 m), suggesting that the conceptual model developed is plausible. However, there's a lot of opportunity for improvement of the numerical model. Improving the spatial and temporal coverage of the existing datasets (more monitoring wells, stream gauges), adding new relevant datasets that weren't available at the time of this study (groundwater extraction or pumping rates, in-situ evapotranspiration estimates), as well as different, concurrent sources of information (geophysical surveys, core sampling and pumping tests, chloride mas balance and water table fluctuation methods for recharge, water quality and tracer studies, etc.) can considerably reduce the uncertainty of the numerical model.

6. BIBLIOGRAPHY

Batlle-Aguilar, J., Banks, E., Batelaan, O., Kipfer, R., Brennwald, M., Cook, P., 2017, 'Groundwater residence time and aquifer recharge in multilayered, semi-confined and faulted aquifer systems using environmental tracers', *Journal of Hydrology*, 546, pp. 150–165. doi:10.1016/j.jhydrol.2016.12.036.

Bresciani, E., Batelaan, O., Banks, E.W., Barnett, S.R., Batlle-Aguilar, J., Cook, P.G., Costar, A., Cranswick, R.H., Doherty, J., Green, G., Kozuskanich, J., Partington, D., Pool, M., Post, V.E.A., Simmons, C.T., Smerdon, B.D., Smith, S.D., Turnadge, C., Villeneuve, S., Werner, A.D., White, N., Xie, Y., 2015a, Assessment of Adelaide Plains Groundwater Resources, Goyder Institute for Water Research Technical Report Series No. 12/x, Adelaide, South Australia.

Bresciani, E., Batelaan, O., Banks, E.W., Barnett, S.R., Batlle-Aguilar, J., Cook, P.G., Costar, A., Cranswick, R.H., Doherty, J., Green, G., Kozuskanich, J., Partington, D., Pool, M., Post, V.E.A., Simmons, C.T., Smerdon, B.D., Smith, S.D., Turnadge, C., Villeneuve, S., Werner, A.D., White, N., Xie, Y., 2015b, Assessment of Adelaide Plains Groundwater Resources: Summary Report, Goyder Institute for Water Research Technical Report Series No. 15/31, Adelaide, South Australia

Bresciani, E., Cranswick, R., Banks, E., Batlle-Aguilar, J., Cook, P., Batelaan, O., 2018, 'Using hydraulic head, chloride and electrical conductivity data to distinguish between mountain-front and mountain-block recharge to basin aquifers', *Hydrology and Earth System Sciences*, 22(2), pp. 1629–1648. doi:10.5194/hess-22-1629-2018.

Department for Environment and Water, 2016, Surface Soil Texture, Dataset Number 1066, Government of South Australia https://data.sa.gov.au/data/dataset/surface-texture

Doherty, J.E., Hunt, R.J., 2010, Approaches to highly parameterized inversion—A guide to using PEST for groundwater-model calibration: U.S. Geological Survey Scientific Investigations Report 2010–5169.

Fitts, C. R., 2012, 'Chapter 3 Principles of Flow', in Groundwater Science. United States: Elsevier Science & Technology. p. 49.

Gallant, J., Dowling, T., Read, A., 2009, 1 second SRTM Level 2 Derived Digital Elevation Model v1.0. Geoscience Australia, Canberra. https://pid.geoscience.gov.au/dataset/ga/69816

Geoscience Australia, 2006, GEODATA TOPO 250K Series 3 - (Personal Geodatabase format). Geoscience Australia, Canberra https://pid.geoscience.gov.au/dataset/ga/63999 (river shapefile)

Geoscience Australia, 2014, Bathymetry GA 2009 9sec v4. Bioregional Assessment Source Dataset. Viewed 22 January 2024, http://data.bioregionalassessments.gov.au/dataset/60fb8bf5-b97d-49c9-b7fb-e7d594d2c75b

Government of South Australia, 2022, Water Security Statement 2022: Water for Sustainable Growth, Department for Environment and Water, https://cdn.environment.sa.gov.au/environment/docs/Final-Water-Security-Statement_150222-PDF_2022-02-18-054712_ithg.pdf

Government of South Australia, Water Data SA, Department for Environment and Water https://water.data.sa.gov.au/Data/Map/ (stream gauge data)

Government of South Australia, WaterConnect groundwater database, https://www.waterconnect.sa.gov.au/Systems/GD/Pages/Default.aspx

Guerschman, J.P., McVicar, T.R., Vleeshower, J, Van Niel, T.G., Peña-Arancibia, J.L., Chen, Y., 2022, Estimating actual evapotranspiration at field-to-continent scales by calibrating the CMRSET algorithm with MODIS, VIIRS, Landsat and Sentinel-2 data, Journal of Hydrology, Volume 605, 2022, 127318, doi:10.1016/j.jhydrol.2021.127318.

Guo, W., Langevin C.D., 2002, 'User's Guide to SEAWAT: A Computer Program for Simulation of Three-Dimensional Variable-Density Ground-Water Flow.' U.S. Geological Survey, 6-A7.

Harbaugh, A.W., 1990, A computer program for calculating subregional water budgets using results from the U.S. Geological Survey modular three-dimensional ground-water flow model: U.S. Geological Survey Open-File Report 90-392, 46 p., https://doi.org/10.3133/ofr90392.

Jeffrey, S.J., Carter, J.O., Moodie, K.B. and Beswick, A.R., 2001, *Using spatial interpolation to construct a comprehensive archive of Australian climate data*, Environmental Modelling and Software, Vol 16/4, pp 309-330. DOI: 10.1016/S1364-8152(01)00008-1. Available online https://www.sciencedirect.com/science/article/abs/pii/S1364815201000081?via%3Dihub (Rainfall SILO data download https://www.longpaddock.qld.gov.au/silo/gridded-data/)

Munro, J., 2017, Wakefield River Catchment Action Plan, Natural Resources Northern and Yorke, Government of South Australia https://cdn.environment.sa.gov.au/landscape/docs/ny/wakefield_river_catchment_action_plan.pdf

Niswonger, R.G., Panday, S., Ibaraki, M., 2011, MODFLOW-NWT, A Newton formulation for MODFLOW-2005: U.S. Geological Survey Techniques and Methods 6-A37, 44 p., https://doi.org/10.3133/tm6A37

Partington, D., *et al.* 2024, National Water Grid Authority: "Further sustainable expansion of irrigated agriculture along the Northern Adelaide Corridor" Milestone 1 Report, unpublished.

Pollock, D.W., 2012, User Guide for MODPATH Version 6—A Particle-Tracking Model for MODFLOW: U.S. Geological Survey Techniques and Methods 6–A41, 58 p.

Shah, N., Nachabe, M., Ross, M., 2007, 'Extinction Depth and Evapotranspiration from Ground Water under Selected Land Covers', *Ground water*. [Online] 45 (3), 329–338.

Smith, M., Fontaine, K., Lewis, S.J., 2015, Regional Hydrogeological Characterisation of the St Vincent Basin, South Australia: Technical report for the National Collaboration Framework Regional Hydrogeology Project. Geoscience Australia Record 2015/16. http://dx.doi.org/10.11636/Record.2015.016

The Goyder Institute for Water Research, 2016, Northern Adelaide Plains Water Stocktake Technical Report, The Goyder Institute for Water Research, Adelaide, South Australia.

Winston, R.B., 2009, ModelMuse—A graphical user interface for MODFLOW–2005 and PHAST: U.S. Geological Survey Techniques and Methods 6–A29, 52 p., available only online at https://pubs.usgs.gov/tm/tm6A29.

Winston, R.B., 2022, ModelMuse version 5.1.1: U.S. Geological Survey Software Release, 15 November 2022, https://doi.org/10.5066/P90QQ94D.